nature COMMUNICATIONS

ARTICLE

Received 24 Jan 2014 | Accepted 2 Oct 2014 | Published 14 Nov 2014

DOI: 10.1038/ncomms6464 OPEN

The role of maternal-specific H3K9me3 modification in establishing imprinted X-chromosome inactivation and embryogenesis in mice

Atsushi Fukuda[1], Junko Tomikawa[2], Takumi Miura[1], Kenichiro Hata[2], Kazuhiko Nakabayashi[2], Kevin Eggan[3], Hidenori Akutsu[1] & Akihiro Umezawa[1]

Maintaining a single active X-chromosome by repressing *Xist* is crucial for embryonic development in mice. Although the *Xist* activator RNF12/RLIM is present as a maternal factor, maternal *Xist* (Xm-*Xist*) is repressed during preimplantation phases to establish imprinted X-chromosome inactivation (XCI). Here we show, using a highly reproducible chromatin immunoprecipitation method that facilitates chromatin analysis of preimplantation embryos, that H3K9me3 is enriched at the *Xist* promoter region, preventing Xm-*Xist* activation by RNF12. The high levels of H3K9me3 at the *Xist* promoter region are lost in embryonic stem (ES) cells, and ES-cloned embryos show RNF12-dependent *Xist* expression. Moreover, lack of Xm-XCI in the trophectoderm, rather than loss of paternally expressed imprinted genes, is the primary cause of embryonic lethality in 70–80% of parthenogenotes immediately after implantation. This study reveals that H3K9me3 is involved in the imprinting that silences Xm-*Xist*. Our findings highlight the role of maternal-specific H3K9me3 modification in embryo development.

[1] Department of Reproductive Biology, National Research Institute for Child Health and Development, 2-10-1 Okura, Setagaya, Tokyo 157-8535, Japan. [2] Department of Maternal-Foetal Biology, National Research Institute for Child Health and Development, 2-10-1 Okura, Setagaya, Tokyo 157-8535, Japan. [3] The Howard Hughes Medical Institute, Harvard Stem Cell Institute and the Department of Stem Cell and Regenerative Biology, Harvard University, 7 Divinity Avenue, Cambridge, Massachusetts 02138, USA. Correspondence and requests for materials should be addressed to H.A. (email: akutsu-h@ncchd.go.jp).

To maintain proper dosage compensation in mammals, one of the two X chromosomes in the female is inactivated[1,2]. In establishment of X-chromosome inactivation (XCI), a large non-coding RNA, *Xist*, is expressed and this non-coding RNA then covers the entire X chromosome in *cis*[1–3]. In mice, two types of XCI occur during female embryonic development. One type involves random XCI, which is observed in cells derived from epiblasts, and one of the two X chromosomes (paternal or maternal) is randomly inactivated. The other involves imprinted XCI (iXCI), which is observed in extra-embryonic tissues and causes XCI of the paternal X chromosome (Xp)[4]. The initiation of iXCI begins at early preimplantation in embryos and Xp-*Xist* is expressed around the four-cell stage[1]. A recent study showed that a maternal factor, the E3 ubiquitin ligase RNF12, is the primary factor responsible for Xp-*Xist* activation[5]. Interestingly, although RNF12 is abundant as a maternal factor in oocytes, Xm-*Xist* is not expressed. Moreover, maternal *Xist* (Xm-*Xist*)-specific imprints, which are refractory to the Xm-*Xist* activation induced by RNF12, are imposed during oogenesis[6]. *Xist* expression analysis using *de novo* DNA methyltransferase (*Dnmt3a/b*) maternal knockout mice demonstrated that *Xist* expression during preimplantation is independent of DNA methylation[7], implying that other epigenetic factors are associated with Xm-*Xist* silencing. However, the nature of these Xm-specific epigenetic modifications is unknown.

A gene-knockout study demonstrated that loss of Xp-*Xist* expression critically affects postimplantation female development due to lack of iXCI, which causes overexpression of X-linked genes in extra-embryonic tissues[8]. Similar to the phenotype observed in Xp-*Xist*-knockout mice, parthenogenetic embryos (PEs) composed of two X chromosomes show increased expression of X-linked genes, as compared with fertilized females, because of the low expression of *Xist*[9]. One of the interesting phenomena observed in PEs is the dramatic developmental failure that occurs immediately after implantation. Around 70–80% of embryos die before embryonic day (E) 9.5, which is the limit of development for PEs[10]. However, it is unknown whether the primary cause of rapid developmental failure in postimplantation PEs is the loss of iXCI or the loss of expression of autosomal paternally imprinted genes[11,12].

The global epigenetic asymmetry of parental genomes in zygotes is retained during early preimplantation phases in mice and changes in gene expression occur in discrete stages to confer totipotency[13,14]. Interestingly, transcriptionally repressive marks, such as histone H3 lysine 9 di-/trimethylation (H3K9me2/3), are specifically imposed on maternal genomes at the zygote stage[13]. Although the regulation of imprinted genes mostly depends on DNA methylation, some imprinted genes are regulated by these histone modifications[15,16]. Thus, Xm-*Xist* silencing machinery may be associated with histone modifications.

Here we reveal that silencing of Xm-*Xist* in preimplantation embryos involves modification of H3K9me3. By using a new chromatin immunoprecipitation (ChIP) method that facilitates chromatin analysis in preimplantation embryos, we show that the *Xist* promoter on the Xm is highly enriched for H3K9me3 at the four-cell stage. This enrichment is lost in the morula and in male embryonic stem (ES) cells. Furthermore, we demonstrate that early loss of H3K9me3 at the *Xist* promoter leads to precocious Xm-*Xist* activation in a Rnf12-dependent manner. Moreover, we demonstrate that establishment of Xm-XCI in the trophectoderm allows PEs to develop at the postimplantation stage without the expression of paternally imprinted genes on autosomes. Therefore, these data indicate that the primary cause of embryonic lethality immediately after implantation in most PEs is loss of XCI rather than loss of the expression of paternally imprinted genes located on autosomes. Our study revealed that silencing of Xm-*Xist* by imprinting to establish iXCI involves H3K9me3, and this finding is expected to resolve the longstanding issues that have limited our general understanding of XCI in mice.

Results

Changes in histone modifications cause Xm-*Xist* derepression. Histone repressive marks, such as H3K9me2/3 and H3K27me3, are specifically imposed on maternal genomes[13]. To investigate the role of maternal-specific modifications in imprinted *Xist* expression, we focused on *Kdm3a* and *Kdm4b*, which encode histone demethylases specific for H3K9me1/2 and H3K9me3 (refs 17,18), respectively. Reverse transcription–PCR analysis showed that oocytes express low levels of *Kdm3a* and *Kdm4b* (Supplementary Fig. 1). Immunofluorescence (IF) analyses revealed that zygotes injected with polyadenylated *Kdm3a* and *Kdm4b* messenger RNAs expressed significantly lower levels of maternal H3K9me2 and H3K9me3, respectively (Fig. 1a–d). Ectopic expression of *Kdm3a* and *Kdm4b* did not affect H3K9me3 or H3K9me2 marks, respectively (Supplementary Fig. 2). We reasoned that if Xm-specific modifications that prevent *Xist* activation were erased by these epigenetic modifiers, Xm-*Xist* would be expressed at the four-cell stage, which is when Xp-*Xist* expression commences.

To facilitate analysis of Xm-*Xist* expression, we used PEs (Fig. 1e). PEs possess two copies of Xm, and Xm-*Xist* is never expressed at the four-cell stage[19]. Xm-*Xist* expression in four-cell PEs, cultured for 48 h, was determined using quantitative real-time PCR (qPCR). Consistent with a previous report[19], Xm-*Xist* was not detectably expressed in most intact (not injected) PEs and PEs injected with *Egfp* mRNA (*Egfp*-PEs; Fig. 1f). Approximately 75% of PEs injected with *Kdm3a* mRNA (*Kdm3a*-PEs) did not detectably express *Xist*. However, Xm-*Xist* expression was detected in all PEs injected with *Kdm4b* mRNA (*Kdm4b*-PEs;

Figure 1 | Alterations in histone modifications derepress Xm-*Xist* expression. (**a**–**d**) Oocytes injected with *Kdm3a* (**a**,**b**), *Kdm4b* (**c**,**d**) or *Egfp* mRNAs were subjected to ICSI. After 7–8 h, embryos were fixed and analysed for H3K9me2 (**a**) and H3K9me3 (**c**) using IF. Nuclei stained with 4′,6-diamidino-2-phenylindole (DAPI) are shown in blue. Representative images are presented on the left. The box-and-whisker plot shows the ratio of maternal to paternal signal intensities. The horizontal line indicates the median. The *P*-values were calculated using the Mann–Whitney *U*-test (*U*-test). Pb, polar body; *n*, number of embryos analysed (**b**,**d**). (**e**) Schema of the generation of PEs with altered histone modifications. To examine the effects of histone demethylation on Xm-*Xist* expression, either H3K9me2 demethylase (*Kdm3a*) or H3K9me3 demethylase (*Kdm4b*) mRNAs were injected into MII oocytes that were then activated. To assess the effects of inhibition of histone deacetylation on Xm-*Xist* expression, oocytes were activated and incubated in the presence of TSA for 24 h. After 48 h, ten four-cell PEs were pooled and analysed as one biological replicate using qPCR. (**f**) Analysis of Xm-*Xist* expression at the four-cell stage. The expression level of Xm-*Xist* in female embryos derived from IVF was defined as 1. One or two asterisks indicate Xm-*Xist* expression in one or two replicates, respectively. The *P*-values were determined using Student's *t*-tests. Error bars indicate the mean ± s.e.m. (**g**–**i**) *Xist* FISH analysis of *Kdm4b*- and *Egfp* + TSA-PEs at the four-cell stage. (**g**) Representative images of FISH results. (**h**) Ratio of cells with *Xist* signal to the total number of cells. *n*, number of interphase cells analysed. (**i**) Ratio of cells with biallelic expression to total cells. The detailed FISH results are shown in Supplementary Table 1. Scale bars, 20 μm.

Fig. 1f), suggesting that H3K9me3 demethylation caused Xm-*Xist* derepression.

We next assessed the effects of a histone deacetylase inhibitor, trichostatin A (TSA), on Xm-*Xist* expression. TSA-treated PEs (Intact + TSA-PEs and *Egfp* + TSA-PEs) also activated Xm-*Xist* (Fig. 1f). No significant changes were detected in Xm-*Xist* expression levels between *Kdm4b*-PEs and *Egfp* + TSA-PEs. However, although co-injection with *Kdm4b* and *Kdm3a* mRNAs did not increase Xm-*Xist* expression levels as compared with *Kdm4b*-PEs, a combination of TSA and *Kdm4b*-mRNA significantly increased Xm-*Xist* expression as compared with *Egfp* + TSA-PEs (2.9-fold, $P < 0.04$, Student's *t*-test; Fig. 1f). Moreover, derepression of Xm-*Xist* transcription occurred in the absence of *Rnf12* overexpression (Supplementary Fig. 3), and *Jpx* and *Ftx*,

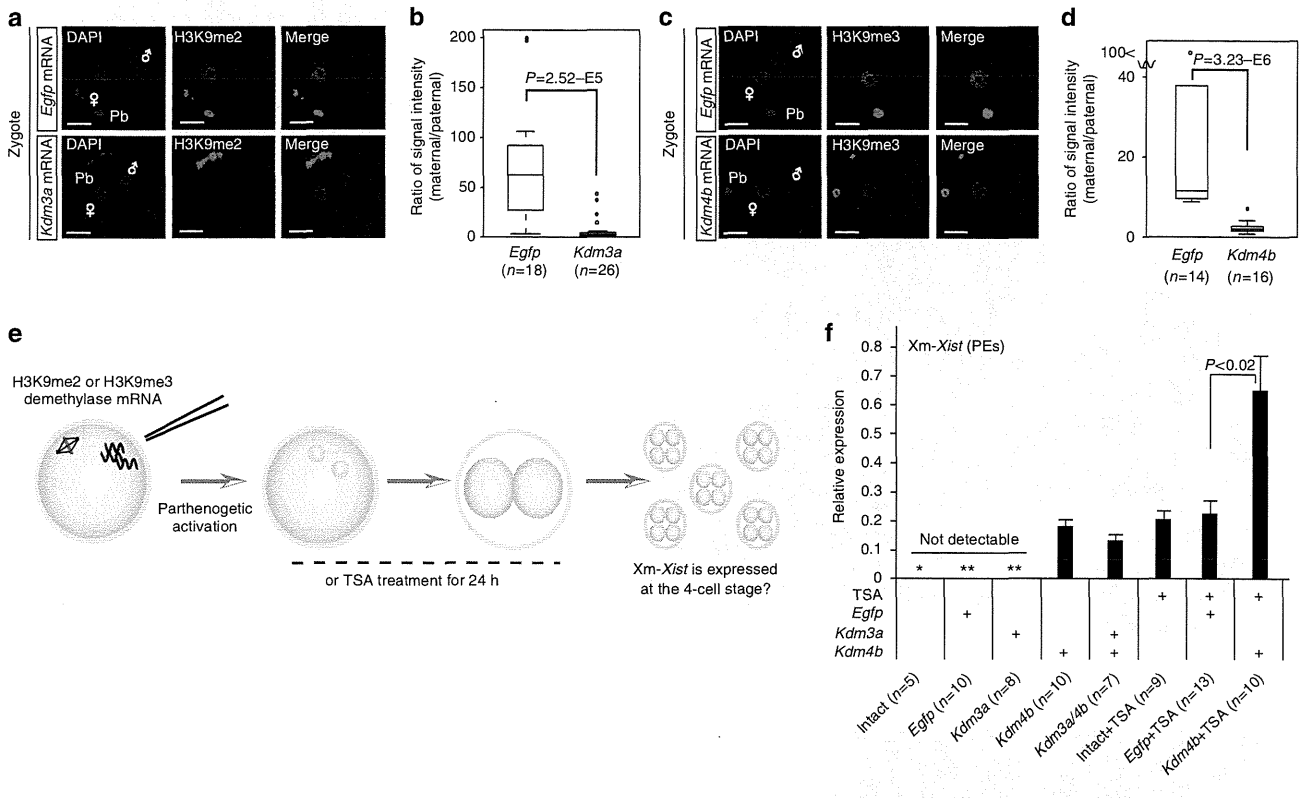

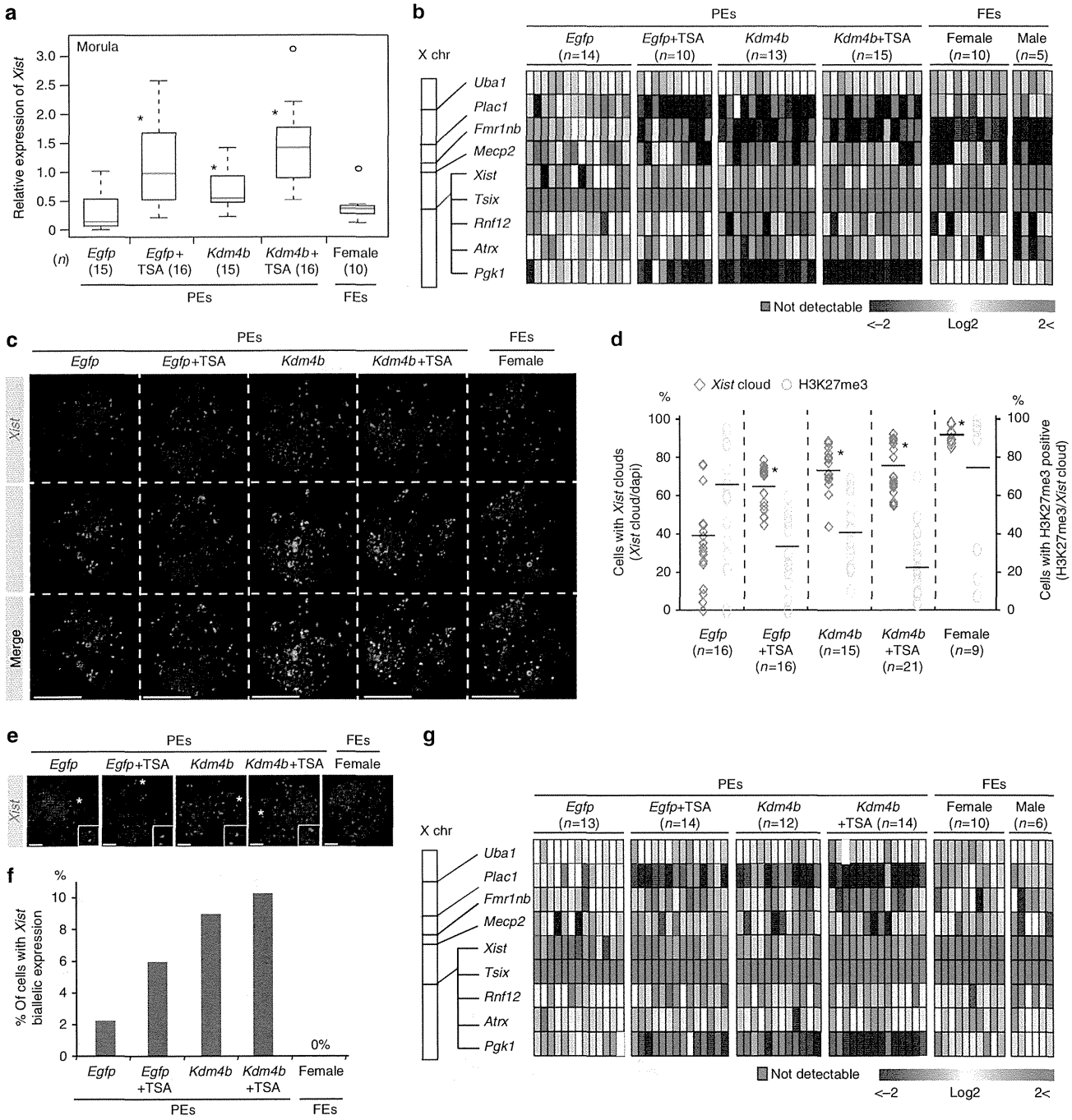

Figure 2 | Global XCI and *Xist* expression states of Xm at late preimplantation stages. (**a**) Analysis of *Xist* expression using qPCR of individual embryos in the morula. An asterisk indicates $P<0.05$ (Student's *t*-test) compared with *Egfp*-PEs. FEs, fertilized embryos. (**b**) Large-scale qPCR analysis of *Xist* and eight X-linked genes in individual blastocysts after culturing for 96 h. Coloured bars indicate expression levels. (**c**,**d**) IF (H3K27me3, green) combined with RNA FISH (*Xist*, red) analysis in 96-h blastocyst stage. 4′,6-diamidino-2-phenylindole (DAPI)-stained nuclei are shown in blue. (**c**) Representative confocal projection. Scale bars, 50 μm. (**d**) The graph shows *Xist* expression and H3K27me3 modification states in individual embryos. The horizontal axis indicates the average percentage in the group. *$P<3.1\times10^{-28}$ (Fisher's exact test). *n*, number of embryos analysed. (**e**,**f**) Xm-*Xist* biallelic expression states in PEs at 96 h. The asterisk indicates cells with biallelic expression. Scale bars, 20 μm. (**f**) Summary of the ratio of biallelic cells to *Xist*-positive cells in 96-h blastocyst stage in each group. The number of cells is shown in Supplementary Table 3. (**g**) qPCR analysis of *Xist* and eight X-linked genes in individual blastocysts after culturing for 120 h. (**h**,**i**) IF (H3K27me3, green) combined with RNA FISH (*Xist*, red) analysis in 120 h blastocysts. *$P<5.4\times10^{-23}$ (Fisher's exact test). Scale bars, 50 μm. (**j**) The ratio of biallelic cells to *Xist*-positive cells in 120 h blastocysts. In qPCR analysis, the average expression level of Xm-*Xist* in *Egfp*-PEs was set as 1 (also see the Methods section). *Gapdh* and *β-actin* were used as internal controls. Data are summarized in Supplementary Table 4.

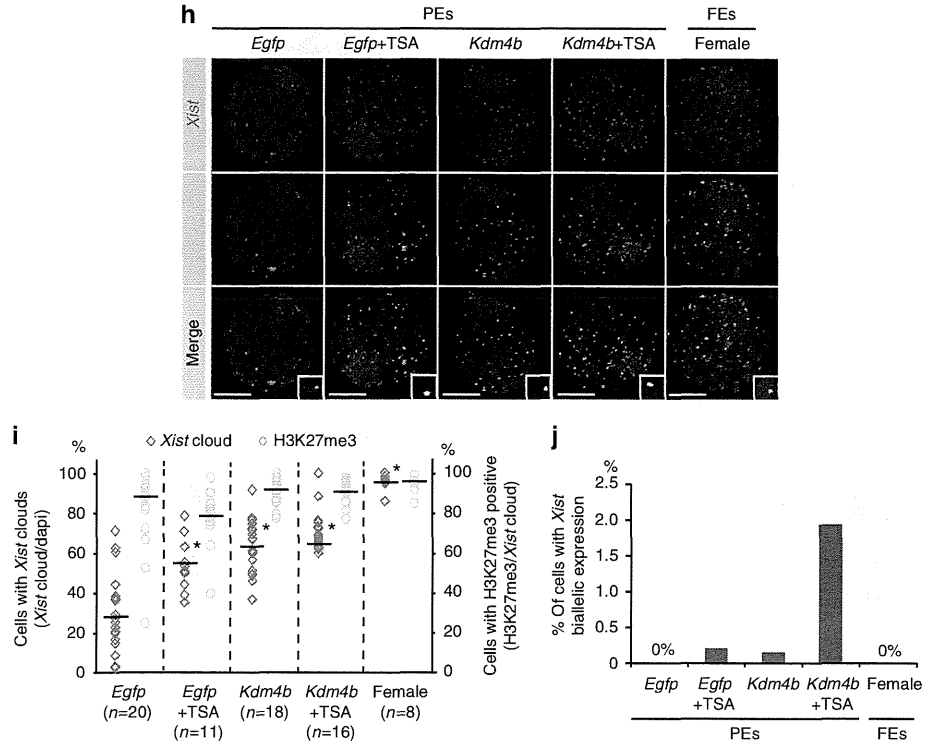

Figure 2 | Continued.

which have been identified as *Xist* activators[2], were not expressed at the four-cell stage. These results showed that KDM4B- and TSA-mediated Xm-*Xist* derepression was not involved in the abnormal expression of known *Xist* activators.

Next, we examined Xm-*Xist* derepression states at the single-cell level by fluorescence *in situ* hybridisation (FISH) of *Xist* RNA. Consistent with the qPCR results, Xm-*Xist* signals were significantly increased in *Egfp* + TSA- and *Kdm4b*-PEs (Fig. 1g,h and Supplementary Table 1). However, neither TSA treatment nor *Kdm4b* overexpression consistently activated Xm-*Xist* in all cells (Fig. 1g,h). FISH analysis also revealed *Xist* biallelic cells in *Kdm4b*- and *Egfp* + TSA-PEs (*Kdm4b*-PEs: 34% and *Egfp* + TSA-PEs: 13%; Fig. 1g,i). Taken together, these results indicated that *Kdm4b* overexpression and TSA treatment induced Xm-*Xist* derepression at the same developmental stage as Xp-*Xist* activation.

Xm-*Xist* transcripts establish XCI at the blastocyst stage. To investigate whether Xm-*Xist* transcripts from the four-cell stage induced XCI in late preimplantation stages, we cultured *Kdm4b*-, *Egfp* + TSA- and *Kdm4b* + TSA-PEs until the blastocyst stage. Development into blastocysts occurred in >80% of PEs in all groups (Supplementary Table 2). At the morula stage (72 h), although *Egfp*-PEs initiated Xm-*Xist* expression, the levels of *Xist* expression were significantly lower compared with those in *Kdm4b*-injected and/or TSA-treated PEs (Fig. 2a). At the 96-h blastocyst stage, we examined the expression levels of *Xist* and X-linked genes (*Tsix*, *Rnf12*, *Pgk1*, *Fmr1nb*, *Atrx*, *Uba1*, *Mecp2* and *Plac1*) in individual embryos. The significant upregulation of *Xist* observed in PEs that had been injected with *Kdm4b* mRNA and/or TSA continued in 96-h blastocyst stage (Fig. 2b). In PEs exhibiting Xm-*Xist* upregulation, *Tsix* expression was not detectable and *Rnf12* was not overexpressed as compared with *Egfp*-PEs (Fig. 2b). The average expression levels of *Pgk1*, *Plac1* and *Fmr1nb* in *Kdm4b*-overexpressing or TSA-treated PE groups were significantly reduced (Supplementary Fig. 4a). However, single embryos in the same group exhibited heterogeneity in the expression levels of these targets (Fig. 2b). Moreover, although Xm-*Xist* was not overexpressed in *Kdm4b*-overexpressing or TSA-treated PE groups compared with levels seen in female fertilized embryos (FEs), the levels of *Plac1* and *Pgk1* were strongly downregulated in *Kdm4b*-, *Egfp* + TSA- and *Kdm4b* + TSA groups (Fig. 2b). These results suggested that Xm-*Xist* expression states differed at the single-cell level in individual embryos.

To gain further insights into *Xist* expression states and repression of X-linked genes on Xm alleles, we conducted IF to detect the H3K27me3 state, which is a hallmark of XCI[20], and performed *Xist* FISH analysis. The *Xist* RNA FISH probe recognizes *Xist* and *Tsix*. Therefore, the cloud state of the FISH signal defined *Xist* expression. Consistent with the qPCR results, the number of cells with *Xist* signals increased significantly in all *Kdm4b*-overexpressing or TSA-treated PEs (Fig. 2c and Supplementary Table 3). However, in all *Kdm4b*-overexpressing or TSA-treated PEs, <45% of *Xist* cloud-containing cells had an H3K27me3 signal (Fig. 2c,d and Supplementary Table 3). We also found that *Xist* biallelic cells were present in all PE groups (*Egfp*-PEs: 2.2%, *Egfp* + TSA-PEs: 5.9%, *Kdm4b*-PEs: 9.0% and *Kdm4b* + TSA-PEs: 10.3%; Fig. 2e,f). These results suggested that there were various Xm-*Xist* expression states present at the single-cell level, affecting the heterogeneity of X-linked genes, and that strong suppression of some X-linked genes in *Kdm4b*-overexpressing or TSA-treated PEs could be attributed to biallelic expression of Xm-*Xist*.

As *Kdm4b* overexpression and TSA treatment did not affect the extent of H3K27me3 modification (Supplementary Fig. 5), its acquisition in PEs may have been slightly delayed compared with that in FEs. In support of this notion, the developmental timing of PEs lags behind that of FEs[9]. Therefore, we extended the culture period to 120 h and again performed qPCR, IF and FISH analyses.

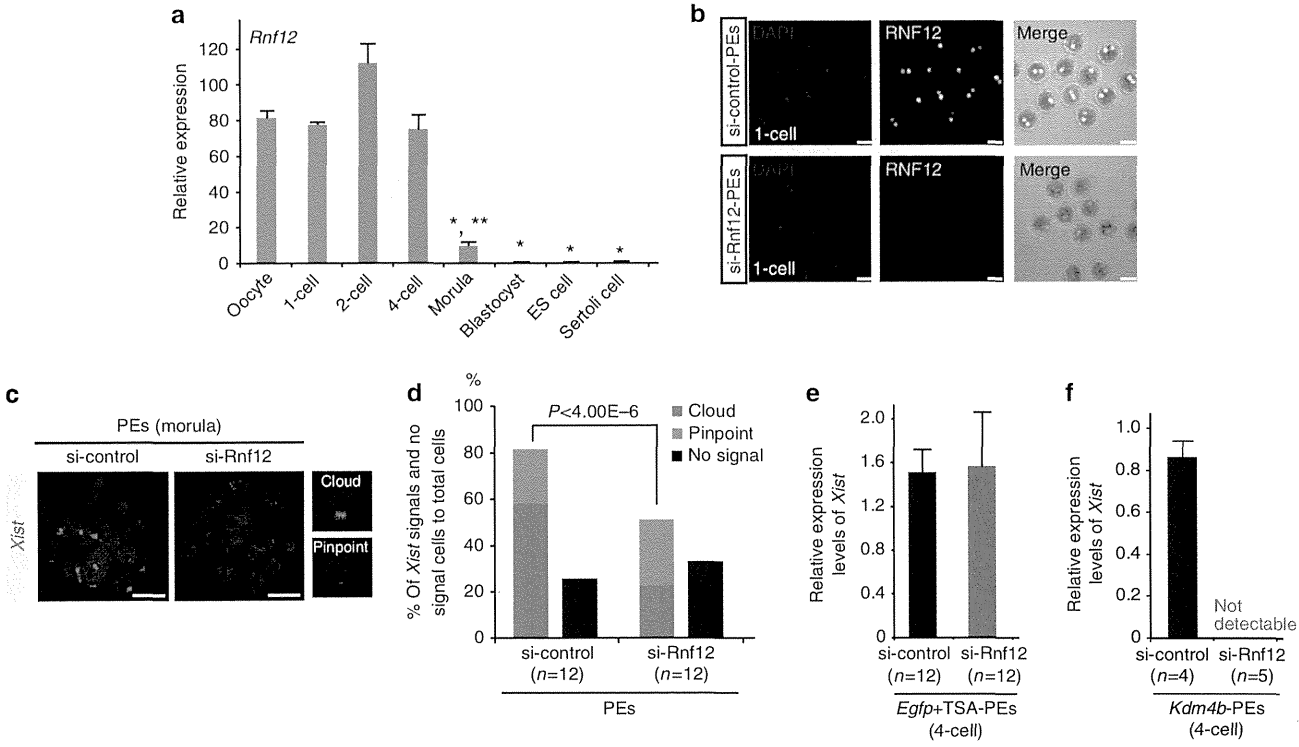

Figure 3 | RNF12 is required for *Xist* expression in various types of preimplantation embryos. (**a**) *Rnf12* expression profiles in preimplantation stages, ES cells and somatic cells. Ten oocytes ($n=3$), ten IVF-1 cells ($n=3$), ten IVF-2 cells ($n=3$) and five IVF-4 cells ($n=3$) were pooled. The expression level of *Rnf12* in the morula stage, as determined using qPCR, represents the average of 16 individual embryos. The numbers of ES and Sertoli cells represent the averages of three independent cell lines and male pups, respectively. The error bars indicate the mean ± s.e.m. $^{*}P<0.004$ compared with oocytes; $^{**}P<0.0001$ compared with ES cells (Student's *t*-test). (**b**) IF analysis of RNF12 at the one-cell stage (green). Samples were fixed 11 h after parthenogenetic activation (18–19 h after siRNA injection). The same laser beam intensities were used to excite the *Rnf12*-knockdown and control samples. 4′,6-diamidino-2-phenylindole (DAPI)-stained nuclei are shown in blue. Two independent experiments were conducted. Scale bars, 50 μm. (**c**,**d**) *Xist* FISH analysis of si-Rnf12 PEs at the morula stage. At 72 h after activation, PEs injected with siRNA were analysed. Representative images of siRNA-treated embryos (**c**). Scale bars, 20 μm. The percentage of total *Xist*-positive signals and -negative cells to total cells in si-Rnf12 and si-control PEs. Biallelic expression was counted as two signals. *n*, number of embryos analysed (**d**). (**e**,**f**) qPCR analysis of Xm-*Xist* expression at the four-cell stage of embryos treated with TSA (**e**) or injected with *Kdm4b* mRNA (**f**). PEs derived from maternal si-Rnf12-treated oocytes. A detailed experimental scheme is shown in Supplementary Fig. 6d. A pool of eight to ten four-cell embryos represents one biological replicate.

As seen in 96-h blastocyst stage, qPCR analysis revealed that *Plac1* and *Pgk1* were significantly repressed in *Kdm4b*-overexpressing or TSA-treated PEs, although heterogeneity was observed (Fig. 2g and Supplementary Fig. 4b). However, *Fmr1nb*, which was significantly repressed in 96-h blastocyst stage of both *Kdm4b*- and TSA-treated groups, did not show marked suppression (Fig. 2g and Supplementary Fig. 4b), suggesting that *Xist* expression states were altered in 120 h blastocysts.

In FISH and IF analysis, a significant increase in the number of *Xist*-positive cells was detected in *Kdm4b*-overexpressing and/or TSA-treated PEs, as compared with *Egfp*-PEs, after culture for 120 h (Fig. 2h,i and Supplementary Table 4). There was a marked increase in the ratio of H3K27me3 spots to cloud *Xist* signals in blastocysts in all groups compared with that observed after 96 h of culture as follows: 88.1% in *Egfp*-PEs, 78.7% in *Egfp* + TSA-PEs, 91.8% in *Kdm4b*-PEs and 91.2% in *Kdm4b* + TSA-PEs (Fig. 2h,i and Supplementary Table 4). Interestingly, >98% of the cells in the *Xist* cloud state exhibited monoallelic *Xist* expression in all groups at 120 h (Fig. 2j).

Taken together, these results indicated that *Kdm4b* overexpression and TSA treatment induced global XCI of Xm in blastocysts and that the counting mechanism automatically functioned in late blastocysts, as has also been observed for Xp alleles[21].

KDM4B-mediated Xm-*Xist* expression depends on RNF12. During preimplantation phases, Xp-*Xist* expression is induced by maternal RNF12 (ref. 5). Thus, we investigated whether Xm-*Xist* expression also depended on RNF12. High *Rnf12* expression levels were maintained until the four-cell stage (around 80-fold higher than in ES cells; Fig. 3a). At the morula stage, although the expression level was significantly decreased compared with that in oocytes, *Rnf12* expression was still more than ninefold higher than that in ES cells (Fig. 3a), indicating that maternal and early zygotic RNF12 may be critical for Xm-*Xist* activation. To examine the dependency of RNF12 on Xm-*Xist* expression, we inhibited maternal and zygotic RNF12 expression using *Rnf12*-siRNA (Supplementary Fig. 6a). IF analysis at the one-cell stage showed a marked decline in RNF12 signal intensity in si-*Rnf12* embryos compared with that in the si-control embryos (Fig. 3b). Significant repression by si-*Rnf12* was maintained in the four-cell stage (Supplementary Fig. 6b,c). Using this knockdown system, we examined whether Xm-*Xist* activation was induced by RNF12 at the morula stage. *Xist* FISH analysis revealed that *Xist* signals (cloud and pinpoint) in PEs treated with si-Rnf12 were significantly reduced at the morula stage as compared with those observed in the controls (si-Rnf12: 50.0% versus si-control: 80.0%; Fig. 3c,d and Supplementary Table 5).

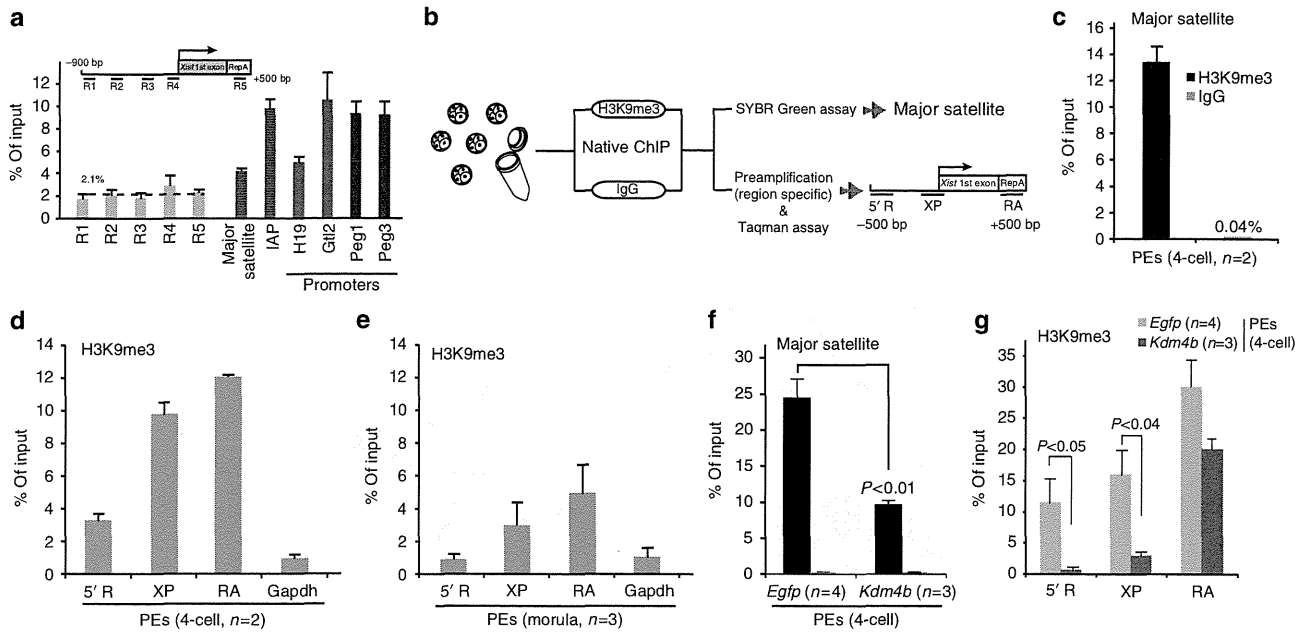

Figure 4 | H3K9me3 states at the Xm-*Xist* promoter region in preimplantation embryos. (**a**) ChIP-qPCR analysis of Xp (sperm) at *Xist* 5′-regions, the *H19*, *Gtl2*, *Peg1* and *Peg3* promoter region, and regions in repetitive elements. $n=2$–4. Rabbit IgG was used as a negative control. The percentage of input for negative control DNA was >1% for all genes tested. The data were not normalized for local nucleosome occupancies. (**b**) Schematic representation of eChIP-qPCR analysis. H3K9me3 states at major satellite regions (**c**) and at *Xist* regions and the *Gapdh* promoter region (**d**) in PEs at the four-cell stage. Two independent experiments were performed. In each experiment, 250 embryos were used. (**e**) H3K9me3 states at the *Xist* and *Gapdh* promoter regions in morula-stage embryos. Three independent experiments were conducted and 40 embryos were used for each assay. H3K9me3 states in major satellite (**f**) and *Xist* regions (**g**) in *Egfp*- and *Kdm4b*-PEs at the four-cell stage. Three (*Kdm4b*-PEs) and four (*Egfp*-PEs) independent experiments were conducted. In each experiment, 170–250 embryos were prepared. The percentages of input for negative controls (IgG) were <0.2% (**f**) and 1.9% (**g**), respectively. Error bars indicate the mean ± s.e.m. The *P*-values were determined using Student's *t*-tests.

Next, we examined whether Xm-*Xist* derepression from the four-cell stage by ectopic *Kdm4b* expression or TSA treatment was regulated by RNF12 (Supplementary Fig. 6d). Four-cell embryos of *Kdm4b*- or *Egfp* + TSA-PEs treated with si-Rnf12 were analysed by qPCR. Depletion of RNF12 did not affect Xm-*Xist* expression in *Egfp* + TSA-PEs compared with the si-control PEs (Fig. 3e), suggesting that factors other than RNF12 may contribute to histone acetylation-mediated Xm-*Xist* activation. This observation is consistent with results obtained using *Rnf12*$^{-/-}$ mice, which demonstrated that *Xist* is activated by RNF12 and other unidentified factors[5,22]. In contrast, *Xist* expression in *Kdm4b*-PEs derived from oocytes treated with si-*Rnf12* did not induce detectable expression of Xm-*Xist* (Fig. 3f). These results demonstrated that KDM4B-mediated Xm-*Xist* expression depended on RNF12 and suggested that H3K9me3 prevented the expression.

Promoter demethylation of H3K9me3 causes Xm-*Xist* derepression. As activation of *Xist* by RNF12 is essential for establishing iXCI[5], we attempted to determine the mechanism responsible for the transcriptional derepression of Xm-*Xist* by KDM4B-mediated demethylation of H3K9me3. We first examined whether H3K9me3 levels were enriched at the Xp-*Xist* promoter region. Nucleosomes were extracted from the sperm genome (Supplementary Fig. 7). ChIP-qPCR revealed the low H3K9me3 levels of Xp-*Xist* in the 5′-regions containing the major promoter for *Xist* expression (average: 2.1%; Fig. 4a), as compared with those of the *H19*, *Gtl2*, *Peg1* and *Peg3* promoter loci (average: 8.5%) and regions in repetitive elements (intracisternal A-particles and major satellite DNAs; average: 7.0%), which are known to be associated with H3K9me3 (ref. 23). These results indicated that the *Xist* promoter region was hypomethylated in sperm, in agreement with Xp-*Xist* being expressed in early embryogenesis.

Preparing sufficient numbers of embryos or oocytes for ChIP combined with deep sequencing (ChIP-seq) analysis is problematic. Some ChIP-qPCR methods requiring small samples have been reported[24]; however, most of these studies are based on a cross-linking ChIP method, in which the ChIP efficiency is lower than that of native ChIP methods[25]. Thus, we developed a new native ChIP method combined with a Taqman qPCR system for quantification of transcription in single cells (termed eChIP-qPCR) and focused on three loci at *Xist* 5′-regions containing the major promoter and repeat A, which is essential for establishment of iXCI[26] (Fig. 4b). We first tested whether the quantification system was biased by using diluted DNA from bulk ES cells. The results of ChIP-qPCR from pre-amplified DNA were comparable to those obtained without pre-amplification (Supplementary Fig. 8).

Using this system, we examined H3K9me3 states at three *Xist* regions and at *Gapdh* promoter regions (as a negative control) in PEs at the four-cell stage. We first investigated whether our eChIP method was efficient by examining major satellite repeats that have been identified as H3K9me3-rich regions in preimplantation embryos[23]. Consistent with a previous report, H3K9me3 was highly enriched at major satellite regions (Fig. 4c). The three *Xist* regions were also highly methylated compared with the *Gapdh* promoter region, as follows: 5′-R, 3.7-fold upregulated; XP, 9.8-fold upregulated; RA, 12.1-fold upregulated; (Fig. 4d).

As Fig. 2a showed Xm-*Xist* spontaneous derepression at the morula stage, we next investigated whether H3K9me3 levels at the *Xist* promoter region were low at this stage. eChIP-aPCR

analysis revealed that enrichment of H3K9me3 was markedly reduced compared with that at the *Gapdh* promoter region in the four-cell stage (5′-R, 0.83-fold upregulated; XP, 2.85-fold upregulated; RA, 4.8-fold upregulated; Fig. 4e). These results suggested that demethylation at the promoter region was essential for Xm-*Xist* derepression.

We then asked whether *Xist* promoter demethylation was involved in the Xm-*Xist* derepression observed in *Kdm4b*-PEs at the four-cell stage. The H3K9me3 levels at major satellite regions in *Kdm4b*-PEs were significantly reduced compared with those in *Egfp*-PEs (*Kdm4b*-PEs: 9.74% versus *Egfp*-PEs: 24.63%, $P<0.01$, Student's *t*-tests; Fig. 4f). At three *Xist* regions, the H3K9me3

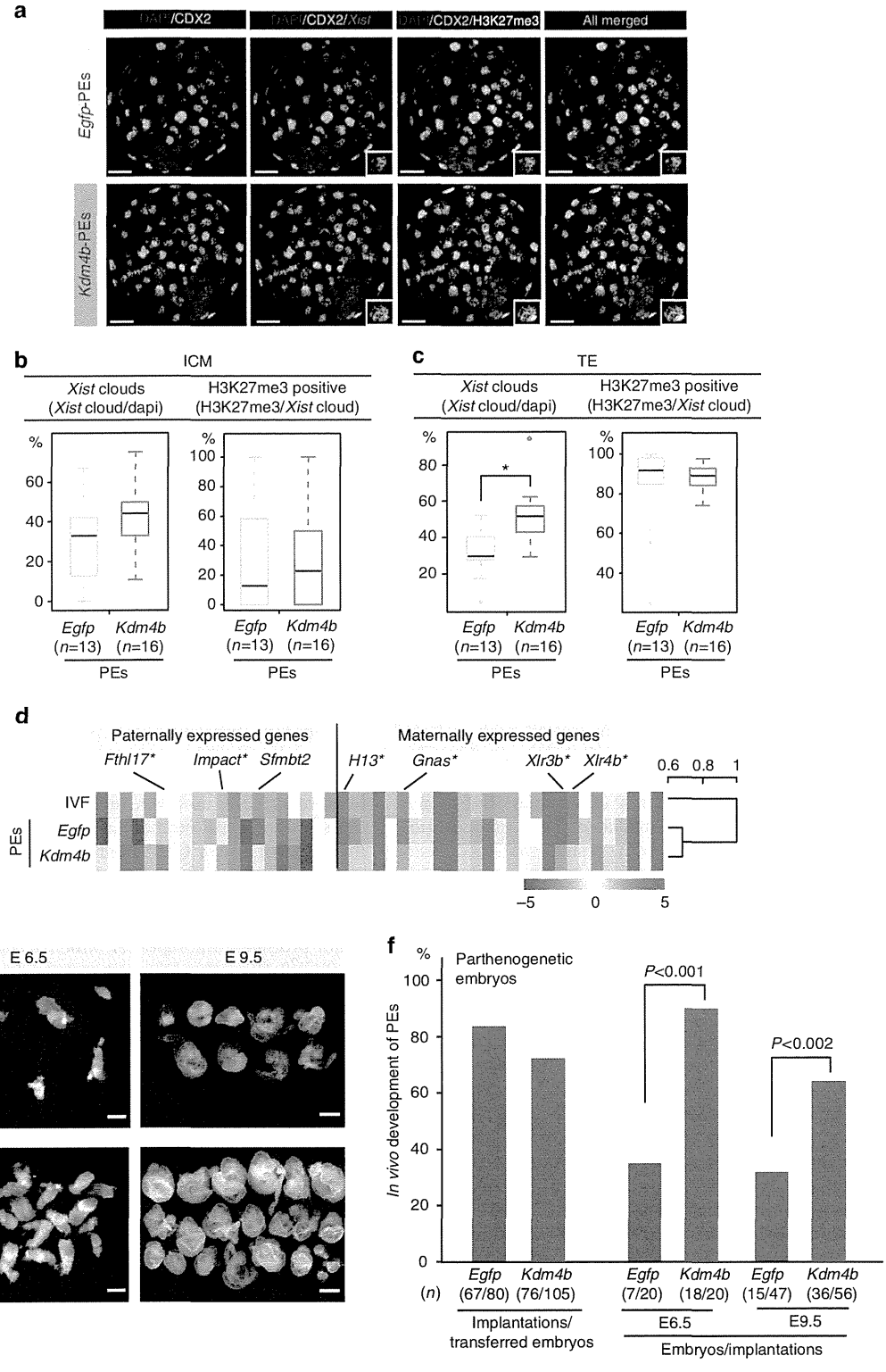

Figure 5

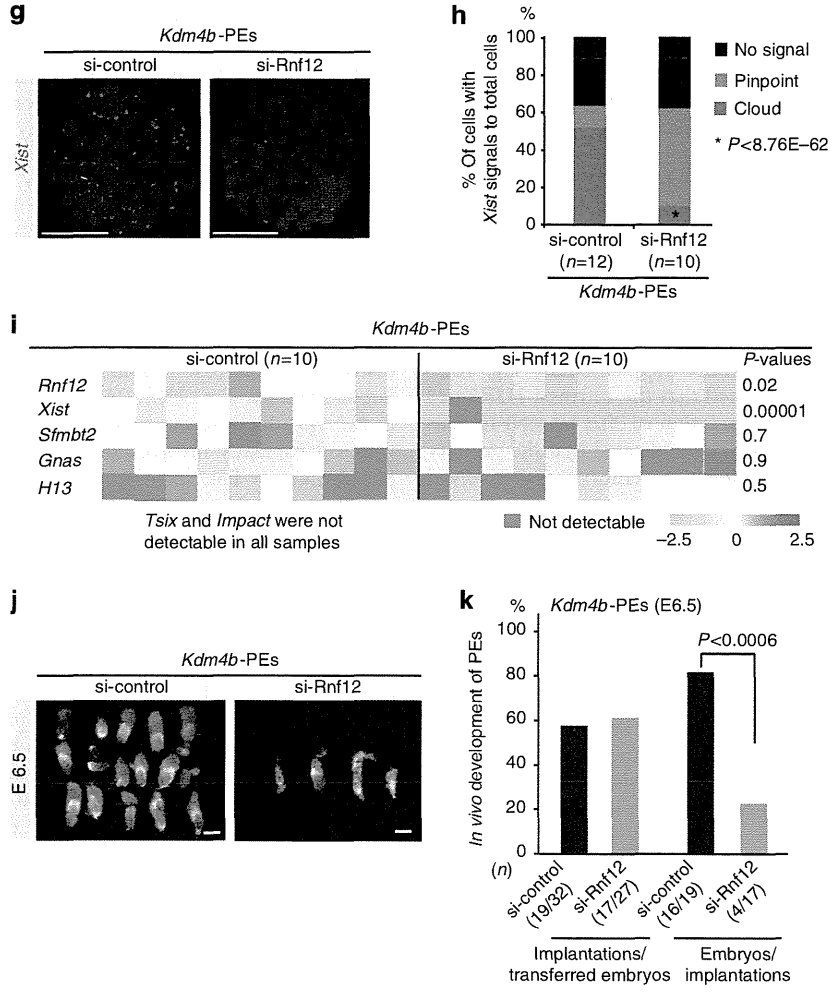

Figure 5 | Loss of Xm-XCI is the primary cause of developmental failure immediately after implantation in most PEs. (**a**) IF combined with FISH analysis of blastocysts in *Egfp*-PEs (upper panel) and *Kdm4b*-PEs (lower panel). CDX2-positive cells were identified as belonging to the trophectoderm (TE). Representative pictures of Z-sections. 4′,6-diamidino-2-phenylindole (DAPI) (blue), CDX2 (green), *Xist* (red) and H3K27me3 (white). Scale bars, 20 μm. The rates of cells with *Xist* (left) or H3K27me3 (right) in the inner cell mass (ICM) (**b**) and TE (**c**), respectively. *n*, number of embryos analysed. The number of cells analysed is shown in Supplementary Table 7. $^{*}P<4.3\times10^{-23}$ (Fisher's exact test). (**d**) Expression states and clustering analysis of imprinted genes. *Sfmbt2* important for placentation and differentially expressed genes (asterisk) are shown. The scale bar indicates normalized values of $\log_2$. (**e**) Embryos with extra-embryonic tissues at E6.5 and E9.5 for *Kdm4b*- and *Egfp*-PEs, respectively. Upper and lower images indicate *Egfp*- and *Kdm4b*-PEs, respectively. Left and right column sides show E6.5 and E9.5, respectively. Scale bars, 200 μm (E6.5) and 500 μm (E9.5). (**f**) Summary of the developmental abilities of *Kdm4b*-PEs and *Egfp*-PEs at postimplantation stages (E6.5 and E9.5). Five and 12 independent recipients were analysed at E6.5 and E9.5, respectively. (**g**,**h**) *Xist* analysis in *Rnf12*-knockdown and control *Kdm4b*-PEs. Representative images of FISH analysis. Scale bars, 50 μm (**g**) and *Xist* expression states (**h**). (**i**) Expression of imprinted and X-linked genes in *Rnf12*-knockdown and control *Kdm4b*-PEs. *P*-values were determined using Student's *t*-tests. (**j**) Embryos with extra-embryonic tissues at E6.5 in *Rnf12*-knockdown and control *Kdm4b*-PEs. Scale bars, 200 μm. (**k**) Summary of the developmental ability of *Rnf12*-knockdown and control *Kdm4b*-PEs at E6.5. Five independent recipients were analysed. The *P*-values were determined using Fisher's exact test.

levels of the promoter region in *Kdm4b*-PEs were significantly reduced, as follows: 5′-R, *Kdm4b*-PEs: 0.84% versus *Egfp*-PEs: 11.48%, $P<0.05$, Student's *t*-tests; XP, *Kdm4b*-PEs: 3.13% versus *Egfp*-PEs: 16.08%; $P<0.04$, Student's *t*-tests; and RA, *Kdm4b*-PEs: 20.16% versus *Egfp*-PEs: 29.99%; Fig. 4g. Taken together, these results demonstrated that H3K9me3 at the promoter region protected Xm-*Xist*, preventing RNF12-mediated activation from the four-cell stage. We concluded that silencing of Xm-*Xist* by imprinting to establish iXCI involved H3K9me3.

Maternal repressive H3K9me3 mark is absent in ES cells. Previous studies have shown that *Xist* is ectopically expressed in embryos cloned from somatic and ES cells[27,28]. However, the cause of aberrant *Xist* expression in cloned embryos remains unknown. Given that high H3K9me3 levels at the promoter region in PEs are lost during development (Fig. 4d,e), we investigated whether the maternal repressive H3K9me3 mark was lost in ES cells and whether *Xist* in ES cells was permissive against RNF12 during oocyte-mediated reprogramming.

To test this possibility, we first examined H3K9me3 states at *Xist* regions in various types of male ES cells, using published data[29,30]. The levels of H3K9me3 at *Xist* regions containing promoters in TT2 and E14 ES cell lines were low compared with those in positive control regions (Supplementary Fig. 9). ChIP-seq analysis revealed that although ectopic expression of KDM4B

in male ES cells induced global H3K9me3 demethylation (Supplementary Fig. 10a–d), it did not alter H3K9me3 levels at *Xist* regions. Moreover, these levels were low compared with those of a known H3K9me3-rich region (Supplementary Fig. 10e)[16]. Furthermore, the expression of *Xist* in cloned embryos was also not affected by ectopic expression of KDM4B (Supplementary Fig. 10f). These results indicated that the maternal repressive H3K9me3 mark was lost.

To establish whether RNF12 is involved in *Xist* activation during oocyte-mediated reprogramming, oocytes treated with si-*Rnf12* were used as recipients for nuclear transfer (Supplementary Fig. 10g). At the four-cell stage, derepression of *Xist* transcription in ES-cloned embryos depended on RNF12 (>50% repression in si-*Rnf12* group; Supplementary Fig. 10h). Taken together, these data indicated that the intrinsic H3K9me3 mark, which was essential for repression of *Xist* by RNF12, was lost during embryo development. This indicated that the primary cause of aberrant *Xist* expression in cloned embryos was involved in loss of intrinsic H3K9me3 at *Xist* regions.

Effects of iXCI disruption on FEs. The effects of Xm-*Xist* derepression on postimplantation development remain unclear. First, we asked whether ectopic *Kdm4b* expression caused Xm-*Xist* derepression in FEs. *Kdm4b*-FEs developed into blastocysts with high efficiency (>80% of two-cell embryos; Supplementary Table 6). At the 96-h blastocyst stage, *Xist* transcription was derepressed in male *Kdm4b*-FEs, while *Pgk1* and *Plac1* levels were reduced to <13% of those observed in controls (Supplementary Fig. 11a). In female *Kdm4b*-FEs, FISH analysis revealed that there were cells with *Xist* biallelic expression (Supplementary Fig. 11b). Although the expression level was slightly elevated (1.3-fold), X-linked genes were also significantly repressed in female *Kdm4b*-FEs (Supplementary Fig. 11c). These results showed that ectopic Xm-*Xist* derepression caused X-linked gene silencing and elimination of iXCI.

To test the effects of iXCI disruption on postimplantation development, we conducted *in vivo* transplantation experiments. Interestingly, our results demonstrated that XCI on Xm during preimplantation did not affect developmental competence to term (*Kdm4b*-FEs: 63.2% versus *Egfp*-FEs: 53.1%; Supplementary Fig. 11d,e), suggesting that aberrant XCI in preimplantation embryos was restored during postimplantation development, probably through an automatic counting function. These results were consistent with the observation that the developmental competency of embryonic cloned embryos was high, despite the ectopic expression of *Xist* and the occurrence of global XCI (Supplementary Fig. 12)[28,31].

Loss of XCI impairs the postimplantation development of PEs. It is still unknown whether the embryonic lethality observed immediately after implantation in the majority of PEs (around 70–80%) can be attributed to the loss of dysregulation of X-linked genes or to loss of expression of autosomal paternally imprinted genes. Figure 2 showed that the percentage of *Xist*-positive cells in *Kdm4b*-PEs was significantly higher than that in *Egfp*-PEs. Thus, we reasoned that *Kdm4b*-PEs would be suitable for studying this long-standing question.

We first performed a detailed analysis of Xm-XCI states in *Kdm4b*-PEs using IF against H3K27me3 and CDX2, a marker of the trophectoderm, in combination with *Xist* FISH, at the blastocyst stage. This analysis revealed that *Xist*-positive cells were significantly increased in the trophectoderm of *Kdm4b*-PEs, although the ratio of H3K27me3-positive cells was comparable to that of *Egfp*-PEs (Fig. 5a–c and Supplementary Table 7). However, no significant difference was observed in the inner cell mass between groups (Fig. 5a–c and Supplementary Table 7), indicating that loss of H3K9me3 in the maternal genome led to establishment of Xm-XCI as an imprinted Xp-XCI.

Next, we carried out transcriptome analysis in *Egfp*-PEs, *Kdm4b*-PEs and FEs using microarray. Clustering analysis based on gene expression patterns showed that all three groups could be distinguished clearly from each other (Supplementary Fig. 13a). Comparison of transcripts between *Egfp*-PEs and *Kdm4b*-PEs identified transcripts that were significantly differentially expressed: 671 transcripts were upregulated and 711 transcripts were downregulated ($P<0.05$, Student's *t*-test and >1.5-fold changes in *Kdm4b*-PEs). Chromosome distribution analysis showed that upregulated transcripts in *Kdm4b*-PEs were distributed across various chromosomes (2.33–7.23%; Supplementary Fig. 13b). However, downregulated transcripts in *Kdm4b*-PEs were mostly concentrated on the X chromosome, which particularly involved the *Xlr* and *Magea* families (10.26%; Supplementary Fig. 13c–e).

Comparison of the imprinted genes between *Egfp*- and *Kdm4b*-PEs revealed that only six genes were significantly differentially expressed (paternally expressed genes: *Impact* and *Fthl17*; maternally expressed genes: *Gnas*, *H13*, *Xlr3b* and *Xlr4b*; Fig. 5d). Clustering analysis based on the expression of imprinted genes showed that the expression levels in *Kdm4b*-PEs were similar to those in *Egfp*-PEs rather than to those of biparental embryos (Fig. 5d). Thus, H3K9me3 demethylation does not result in restoration of expression states in paternally expressed genes.

We conducted *in vivo* transplantation experiments using *Kdm4b*-PEs. Surprisingly, at E6.5, the developmental rates of *Kdm4b*-PEs were markedly increased compared with those of *Egfp*-PEs (*Kdm4b*-PEs: 90% versus *Egfp*-PEs: 35%; $P<0.001$, Fisher's exact test; Fig. 5e,f). At E9.5, although the stages of the recovered embryos varied, *Kdm4b*-PEs retained a significantly higher developmental ability compared with controls (*Kdm4b*-PEs: 64.3% versus *Egfp*-PEs: 31.9%; $P<0.002$, Fisher's exact test; Fig. 5e,f).

However, we did not rule out the possibility that the significant improvement in *Kdm4b*-PE development resulted from restoration of the expression levels of some imprinted genes. To determine whether the improvement in developmental competency could be attributed to the gain of XCI, we constructed *Kdm4b* + si-*Rnf12*-PEs. In *Kdm4b*-PEs with si-*Rnf12* at the blastocyst stage, *Xist* expression analysis by FISH revealed that *Xist* cloud signals in control *Kdm4b*-PEs were present in 51.9% of cells, while those in *Rnf12*-knockdown *Kdm4b*-PEs were present in only 10% of cells, and most of the signals were pinpoint rather than cloud (Fig. 5g,h and Supplementary Table 8).

qPCR analysis showed that although *Xist* signals were significantly reduced in *Kdm4b*-PEs with si-*Rnf12* (12.5% of the control on average), the expression levels of *Impact*, *H13* and *Gnas*, which are expressed in response to ectopic *Kdm4b* expression (Fig. 5d), did not change when compared with those of controls (Fig. 5i). We further demonstrated that RNF12 depletion did not affect *Tsix* and *Sfmbt2* expression levels in *Kdm4b*-PEs (Fig. 5i). These results clearly indicated that RNF12 depletion led to *Xist* downregulation in *Kdm4b*-PEs, without altering the features of PEs.

Finally, *in vivo* transplantation experiments demonstrated that *Xist* repression by RNF12 depletion significantly inhibited developmental competency at E6.5 in *Kdm4b*-PEs (*Kdm4b* + si-control: 84.2% versus *Kdm4b* + si-*Rnf12*: 23.5%; $P<0.0006$, Fisher's exact test; Fig. 5j,k). Taken together, these results demonstrated that the developmental defects seen in PEs immediately after implantation could be attributed to the lack of XCI, but not to loss of expression of paternally expressed genes.

Discussion

In this study, we demonstrated that maternal imprinting of Xm, which protected against *Xist* activation by RNF12 in the preimplantation stages, was mediated by H3K9me3.

Xm-*Xist* imprints are established during oogenesis and autosomal imprinting also occur in the phases[6,10]. In many imprinted genes, DNA methylation at the promoter regions is the primary regulator and H3K9me3 modifications overlap with these regions[32]. However, it is not clear why Xm-*Xist* regions are targeted by H3K9me3, but not by DNA methylation. One of the possibilities is that during primordial germ cell development, *Xist* must be silenced to activate the inactivated allele before inducing the expression of *Dnmt3a/3l*, which encodes a *de novo* DNA methyltransferase that is activated during oogenesis[33]. Consistent with this concept, *Xist* repression begins in primordial germ cells at E10.5 (ref. 34). Thus, comparison of H3K9me3 states at promoter regions in non-growing oocytes with those in growing oocytes will greatly facilitate understanding of the molecular mechanisms of iXCI.

We found that *Kdm4b*-, *Egfp* + TSA- and *Kdm4b* + TSA-PEs did not show complete XCI at the blastocyst stage as compared with female FEs. These results suggested that other repressive marks were imposed on Xm to silence Xm-*Xist* expression. Alternatively, removal of H3K9me3 may be incomplete because demethylation at RA regions was mild (Fig. 4g). However, it is not clear why RA regions show resistance against demethylation by KDM4B. As suggested in a previous study, this mechanism may be related to the three-dimensional structure of the A-repeat, which has been reported to constitute stable regions in the *Xist* transcript[35]. Further studies using ChIP-seq and/or chromatin-conformation capture sequencing technologies in preimplantation embryos are required for comprehensive understanding of *Xist* regulation.

In ES cells, RNF12 induces *Xist* expression through degradation of REX1, which is required for suppression of *Tsix*[36]. Interestingly, we did not detect *Tsix* expression from the morula to the blastocyst stages in *in vitro*-fertilized (IVF) embryos, implying that the molecular mechanism of RNF12-mediated *Xist* activation differs between imprinted and randomly induced XCI. It is not known whether the role of RNF12 in *Xist* activation during the preimplantation stages was direct or indirect. Recent RNF12 studies reported the specific binding of RNF12 to *Smad7* in mouse ES cells[37], suggesting that signalling via transforming growth factor-β family members may be associated with imprinted *Xist* activation.

In this study, we revealed the molecular mechanisms underlying imprinting of XCI and demonstrated the role of XCI in various types of embryo development in mice. Recent studies using somatic- and ES-cloned embryos revealed that aberrant *Xist* reprogramming is a major cause of developmental failure in cloned embryos[27,28]. We found that RNF12 was highly expressed in oocytes compared with somatic and ES cells (>80-fold). Moreover, we showed that H3K9me3 levels at *Xist* promoter regions were low in ES cells and that *Xist* expression in ES-cloned embryos depended on RNF12. These data provided the first evidence that RNF12 inhibited developmental reprogramming. Therefore, the use of RNF12-depleted oocytes as recipient cells would improve cloning efficiency. However, *Xist* activation in cloned embryos may be induced by factors other than RNF12, as supported by the observation that *Xist* was still expressed at ~40% of control levels, even after marked depletion of RNF12. Consistent with this notion, a recent study has demonstrated that RNF12 is dispensable for random XCI *in vivo*[38].

Xm-*Xist* derepression from the four-cell stage could rescue developmental defects in PEs. This finding demonstrated that the primary cause of developmental failure immediately after implantation was a lack of XCI, but not a lack of expression of paternally imprinted genes. We also tested whether *Kdm4b*-PEs could extend development; however, we did not observe extended *Kdm4b*-PE development after E9.5, implying that expression of paternally imprinted genes is required for subsequent development in PEs[11,12].

Our data resolved several long-standing unanswered questions about XCI during preimplantation in various types of embryos (Supplementary Fig. 14). Moreover, given that injection of *Kdm4b* mRNA into PEs improved their developmental ability, genetic mutation leading to embryonic lethality could be rescued by transient expression of epigenomic modifiers during preimplantation phases.

Methods

Embryo manipulations. All mice were maintained and used in accordance with the Guidelines for the Care and Use of Laboratory Animals of the Japanese Association for Laboratory Animal Science and the National Research Institute for Child Health and Development (NRICHD) of Japan. All animal experiments were performed according to protocols approved by the Institutional Animal Care and Use Committee of the NRICHD (Permit Number: A2006-009).

Adult female B6D2F1 mice were purchased from Clea Japan (Tokyo, Japan) and oocytes were collected following standard methods[27]. PEs were generated using Ca-free M16 medium containing 8 mM $SrCl_2$ and Cytochalasin B (5 μg ml^{-1}) (Sigma-Aldrich, St Louis, MO, USA), and cultured KSOM (EMD Millipore, Darmstadt, Germany). Injection experiments (mRNA, short interfering RNA (siRNA) and nuclear transfer) were conducted using a Prime Tech Piezo drive (Sutter Instrument Company, Novato, CA, USA). To produce cloned embryos, nuclear-transferred oocytes were parthenogentically activated. Manipulated embryos were cultured to the developmental stages, as follows: 4-cell, 48 h; morula, 72 h; and blastocyst, 96 and 120 h after parthenogenetic activation or ICSI, respectively. All embryos were cultured at 37 °C in KSOM in an atmosphere containing 5% CO_2. In the TSA experiment, the embryos were cultured for 24 h in activation and culture media containing 50 nM TSA (Sigma-Aldrich). IVF fertilization and nuclear transfer were performed following published procedures[27]. To determine the effects of ectopic KDM4B expression on *Xist* expression in cloned embryos, doxycycline was added to ES cell culture and KSOM medium to a final concentration of 2 μg ml^{-1}. Pseudopregnant ICR mice (Clea Japan) were used as embryo recipients. At E6.5, E9.5 and E18.5, the embryos were recovered from the uterus.

***In vitro* mRNA synthesis.** The coding region of *Kdm3a* was amplified from mouse testis complementary DNA using PCR with KOD-Plus-Neo DNA polymerase (Toyobo, Osaka, Japan). Forward and reverse primers contained T7 promoter and poly(T)$_{120}$ sequences, respectively. A step-down PCR amplification method was used, following the manufacturer's instructions (Toyobo). Poly(A)-containing PCR products were subjected to *in vitro* transcription using a mMESSAGE mMACHINE T7 ULTRA Kit (Life Technologies, Carlsbad, CA, USA), following the manufacturer's instructions. To generate a *Kdm4b* DNA template for *in vitro* transcription, pCMV-SPORT6 containing the full-length *Kdm4b* mRNA was used as the PCR template (DNAFORM, Kanagawa, Japan, Clone ID 3490671). *Egfp* cDNA was cloned using the pGEM-T Easy Vector System (Promega, Madison, WI, USA) and transcribed *in vitro* using the mMESSAGE mMACHINE T7 ULTRA Kit (Life Technologies) following the manufacturer's instructions. The concentrations of the mRNAs were adjusted to 150 ng ml^{-1} (*Egfp*), 550 ng ml^{-1} (*Kdm3a*), or 450 ng ml^{-1} (*Kdm4b*) to maintain a constant number of injected mRNA molecules. The primer sequences used for generating the templates for *in vitro* transcription are shown in Supplementary Table 9.

***Rnf12* knockdown.** siRNA targeting *Rnf12* (si-Rnf12 sense 5′-GAAGUCAAAUG GAUCGCUUTT-3′ A and antisense 5′-AAAGCGAUCCAUUUGACUUCTG-3′ GC, and the negative control siRNA (si-control: 4390846) were purchased from Life Technologies. The final concentration of each siRNA was 50 ng ml^{-1}. The siRNA was injected into MII oocytes using the Piezo drive and then incubated for 6–7 h in KSOM medium at 37 °C in an atmosphere containing 5% CO_2 before mRNA injection. For the NT experiment using *Rnf12*-knockdown oocytes, oocytes were incubated for 5–6 h after siRNA injection, and NT was then conducted and activated as described above.

Immunofluorescence. Oocytes injected with mRNAs were subjected to ICSI. After 10–11 h, the zygotes were fixed with 2% paraformaldehyde (PFA) in PBS containing 0.1% polyvinyl alcohol (PBS-PVA) for 15 min at room temperature (RT). Zygotes were then permeabilized using 0.2% Triton X-100 in PBS-PVA for 15 min at RT and blocked in 1% BSA in PBS-PVA for 1 h at RT. The primary antibodies used in the assay were as follows: anti-H3K9me3 (ab8898, 1:500 dilution, Abcam, Cambridge, UK), anti-H3K9me2 (ab1220, 1:500, Abcam) and anti-H3K27me3

(07-449, 1:150, EMD Millipore). The primary antibodies were diluted with blocking solution (PBS-PVA containing 1% BSA) and the embryos were incubated overnight at 4 °C. After washing in blocking solution, the embryos were incubated for 1 h at RT with Alexa Flour 634- or 546-conjugated anti-mouse or anti-rabbit IgG secondary antibodies (1:500, Life Technologies). After the embryos were washed, the nuclei were stained with 1 μg ml^{-1} 4′,6-diamidino-2-phenylindole and the embryos were placed on a glass slide and observed with a LSM510 laser scanning confocal microscope (Carl Zeiss, Oberkochen, Germany). Signal intensities of maternal and paternal pronuclei were calculated using NIH ImageJ software (http://rsb.info.nih.gov/ij/).

In *Rnf12*-knockdown experiments, one-cell and four-cell PEs were fixed at 10–11 h (18–19 h after siRNA injection) and 48 h after activation, respectively. Anti-RNF12 (1:500, Abnova, Taipei, Taiwan) and Alexa Fluor 488-conjugated anti-mouse IgG antibodies (1:500, Life Technologies) were used as the primary and secondary antibodies, respectively. *Rnf12*-knockdown and negative-control PEs were observed under the same conditions, to assess knockdown efficiency. Signal intensities were calculated using ImageJ software.

Fluorescent *in situ* hybridization. The zona pellucida of embryos was removed using acid Tyrode solution (Sigma-Aldrich) and then fixed and permeabilized with 2% PFA-PVA containing 0.25% Triton X-100 for 10 min on ice. The samples were placed on glass slides, evaporated to dryness, dehydrated sequentially in 70 and 100% ethanol and then air-dried. Hybridization buffer containing an *Xist* probe (provided by T. Sado) was prepared using a Nick Translation Kit (Abbott, Abbott Park, IL, USA) and Cy3-dUTP (GE Healthcare Life Sciences, Fairfield, CT, USA) and was then applied to the slides. The slides were then incubated and washed as previously described[26]. Fluorescence was visualized using the LSM510.

IF combined with FISH. The zona pellucida of embryos was removed using acid Tyrode solution (Sigma-Aldrich) and fixed with 2% PFA-PVA for 15 min at RT in four-well dishes. The fixed samples were permeabilized with 0.5% Triton X-100 in PBS-PVA for 20 min on ice. After washing with PBS-PVA, the samples were blocked in 1% BSA-PBS-PVA containing 1.3 U ml^{-1} RNaseOUT (Life Technologies) for 30 min at RT. After washing, the embryos were incubated with primary antibodies (anti-CDX2 (BioGenex, San Ramon, CA, USA), diluted 1:30 and anti-H3K27me3 diluted 1:150 in blocking buffer containing 1.3 U ml^{-1} RNaseOUT) for 1 h at RT. Secondary antibody reactions were performed as described above. The samples were placed on glass slides, evaporated to dryness, dehydrated sequentially in 70 and 100% ethanol and air dried. The samples were then analysed by FISH according to the procedures described above.

Analysis of IF combined with FISH data. *Xist* cloud signals detected in three-dimensional images using *Z*-sections of the LSM Image Browser (Carl Zeiss) were judged as positive. Only cells that did not overlap at interphase were used in the analysis. Biallelic expression was defined as cells with two *Xist* cloud spots. Statistical analysis was performed using Fisher's exact test.

Gene expression analysis. Total RNA was extracted using an RNeasy Micro Kit (Qiagen, Venlo, The Netherlands) and treated with DNase following the manufacturer's instructions. mRNAs were reverse transcribed using an oligo(dT) primer and SuperScriptIII Reverse Transcriptase (Life Technologies). For quantitative gene expression analysis with high specificity, TaqMan probes (Life Technologies) were used in all assays. In four-cell stage embryos, *Xist* was assayed in triplicate and only the samples that were detected in two or three replicates were judged as positive. In morulae and blastocysts, expression of target genes was assayed in duplicate. *Gapdh* was used as the internal control in the four-cell-stage assays and *Rnf12* was used in the time-lapse assays. *Gapdh* and *Actb* (encoding β-actin) were used as internal controls at the morula and blastocyst stages. For normalization of qPCR analysis (Fig. 2b,g), the expression levels of all embryos were normalized to the average expression levels of *Egfp*-PEs. The TaqMan probes and primer sets used in this study are shown in Supplementary Table 8.

Generation of *Kdm4b*-inducible ES cell lines and ES cell culture. The XhoI- and ClaI-linearized pGEM-IRES-EGFP plasmids were inserted into the cognate sites of pPB-CAG-EBNX (provided by A. Bradley) to generate pPB-CAG-IRES-EGFP. A Tet3G fragment with BglII and XhoI cleavage sites was amplified from a pEF1a-Tet3G template (Clontech Laboratories, Mountain View, CA, USA) using PCR and inserted into pPB-CAG-IRES-EGFP, generating the vector pPB-CAG-Tet3G-IRES-EGFP. The XhoI and BamHI cleavage sites in pPB-UbC (provided by A. Bradley) were replaced with the p-TRE3G multiple cloning sites (Clontech). The *Kdm4b* coding sequence, with terminal ClaI and BamHI cleavage sites, was amplified by PCR and inserted into the corresponding sites of pPB-TRE3G, yielding pPB-TRE-Kdm4b.

The NCH.4.6 male mouse ES cell line (C57B6/N × C57B6/N), which had a normal karyotype, was electroporated with pPB-TRE-Kdm4b, pPB-CAG-Tet3G-IRES-EGFP and pCMV-hyPBase (provided by A. Bradley). All ES cells used in this study were cultured in knockout DMEM (Life Technologies) containing recombinant human leukemia inhibitory factor culture supernatant for mouse ES cell culture (Wako Pure Chemical Industries, Ltd, Osaka, Japan), as well as GlutaMAX, 2-mercaptoethanol, non-essential amino acids and 15% KSR (all from Life Technologies). Doxycycline (2 μg ml^{-1}; Sigma-Aldrich) was added to ES cell culture medium to induce ectopic KDM4B expression.

Western blotting. Cells were extracted using a stock lysis buffer containing 1 M Tris–HCl, 5 M NaCl, 10% Triton-X and protease inhibitors, and were subjected to *e*-PAGEL (ATTO, Amherst, NY, USA) electrophoresis. The membranes were washed in TBS containing 0.1% Tween 20 (TBS-T) and blocked in 5% skim milk in TBS-T for 1 h. The membranes were incubated with anti-KDM4B antibodies (1:500 dilution; Active Motif, Carlsbad, CA, USA) overnight at 4 °C, washed and incubated with a rabbit horseradish peroxidase-conjugated secondary antibody (1:5,000 dilution; Sigma-Aldrich) for 1 h at RT. Immunoblottings were visualized using SuperSignal chemiluminescent substrate (Thermo Scientific, Waltham, MA, USA) and an ImageQuant LAS4000 system (GE Healthcare). After capturing the images, the membranes were washed with WB Stripping Buffer (Nacalai Tesque, Kyoto, Japan) for 10 min, washed with TBS-T and incubated with an anti-β-actin antibody conjugated to fluorescein isothiocyanate (1:2,000 dilution; Sigma-Aldrich) for 1 h at RT.

ChIP analysis of K4B-ES cells. Trypsinized feeder-free ES cells (2×10^7) were collected and fixed with 1% formaldehyde. The cells were resuspended in SDS lysis buffer (ChIP Reagent, Nippon Gene Co., Ltd.) and the lysate was sonicated to fragment chromatin using a S220 Focused-ultrasonicator (Covaris, Woburn, MA, USA). The chromatin was purified by centrifugation and immunoprecipitated with Protein A-beads (Veritas Life Sciences, Ribeirão Preto, Brazil) conjugated to anti-H3K9me3 antibodies (Abcam: ab8898) or rabbit IgG (Abcam: ab37415) in Buffer A with protease inhibitor (LowCell ChIP kit, Diagenode, Denville, NJ, USA) overnight at 4 °C. The chromatin beads were washed with Buffers A and C (LowCell ChIP kit). After washing, the chromatin beads were incubated in ChIP direct elution buffer (ChIP Reagent) for 6 h at 65 °C, following incubation with 2 μl proteinase K (20 mg0 ml^{-1}) for 2 h at 55 °C. The DNA immunoprecipitated from the supernatant was purified using Agencourt AMPure XP beads (Beckman Coulter, Inc., Pasadena, CA, USA) according to the manufacturer's instructions.

ChIP combined with deep sequencing. ChIP-Seq libraries were prepared using the NEBNext ChIP-Seq Library Prep Master Mix Set and Multiplex Oligos from Illumina (New England BioLabs Inc., Ipswich, MA, USA) according to the manufacturer's instructions. Ten nanograms of ChIP or input DNA was subjected to end repair, dA-tailing and adaptor ligation, and amplified using nine cycles of PCR. The final library size was checked using a 2100 Bioanalyzer (Agilent Technologies, Santa Clara, CA, USA). After the concentration of each library was determined using qPCR with a KAPA Library Quantification Kit-Illumina/Universal system (KK4824, Kapa Biosystems, Wilmington, MA, USA), the libraries were sequenced using the HiSeq 1000 sequencing system (Illumina, San Diego, CA, USA) to generate 100 bp × 2 paired-end data.

ChIP-seq data analysis. Reads from each sample were first trimmed by removing adapter sequences and low-quality bases at ends using Trimmomatic 0.22 (http://www.usadellab.org/cms/index.php?page=trimmomatic). Approximately 115 million reads for each of the ChIP and input libraries were aligned to the mouse reference genome (mm10:http://genome.ucsc.edu/cgi-bin/hgGateway) using the Burrows-Wheeler Aligner 0.6.2. Uniquely mapped reads were selected using a custom script, converted from SAM to BAM format using SAMtools 0.1.18 and processed using Picard 1.83 to mark PCR duplicates. Reads with a mapping quality of <20 were removed using SAMtools 0.1.18. The resulting BAM files (a pair of files for ChIP and input libraries) were visualized using the Integrative Genomics Viewer (http://www.broadinstitute.org/igv/) and subjected to peak detection using the MACS algorithm implemented in Avadis NGS software (Agilent). In scatter plot analysis using 1 and 15 K4B-ES cell lines, the numbers of mapped reads were counted for 10,000-bp windows (with a sliding size of 5,000 bp). To adjust for differences in total amount of reads, the number of mapped reads in each window was transformed into reads per million format. Calculation methods are available on request.

ChIP-qPCR analysis of sperm. Sperm were obtained from BDF1 mice aged 9–12 weeks. Preparation of sperm chromatin was performed according to published protocols with modifications[39,40]. For each native ChIP experiment, 5×10^7 sperm were used. Sperm were washed twice with PBS. The pellet was suspended in PBS containing 0.5% Triton-X, 10 mM dithiothreitol (DTT) and protease inhibitor (Diagenode), and incubated on ice for 1.5 h. After washing with PBS, pelleted sperm nuclei were suspended in 400 μl PBS containing 1 mM $CaCl_2$ and 1 mM DTT, and incubated for 5 min at 37 °C. After incubation, 1 μl (2×10^6 gel units per ml) micrococcal nuclease (New England BioLabs) was added to the nuclei, which were then incubated for 5 min at 37 °C. EDTA was added to a concentration of 0.5 mM and solubilized chromatin was clarified by centrifugation for 15 min at 15,000 r.p.m. at 4 °C. The pellets were suspended in PBS containing $CaCl_2$ and DTT (at the same concentrations as used above), and treated again with micrococcal nuclease. To examine whether H3K9me3-modified nucleosomes were

present in sperm chromatin, soluble (chromatin) and insoluble (pellet) fractions were subjected to western blotting using anti-H3K9me3 antibodies (ab8898; 1:1,000), as described above.

Chromatin was incubated with Protein A beads conjugated to anti-H3K9me3 antibodies (ab8898) or rabbit IgG (ab37415) overnight at 4 °C in ChIP buffer (40 mM Tris–HCl, pH 7.5, 1 M NaCl and 10 mM EDTA). Pelleted beads were washed twice with Buffer 1 (50 mM Tris–HCl, pH 7.5, 500 mM NaCl and 10 mM EDTA) and Buffer 2 (50 mM Tris-HCL, pH 7.5, 300 mM NaCl and 10 mM EDTA). The pelleted beads were suspended in ChIP direct elution buffer and incubated with proteinase K for 2 h at 37 °C. The immunoprecipitated DNA was then purified using Agencourt AMpure XP beads.

ChIP-qPCR analysis was performed according to published methods using SYBR Green[39]. The sequences of each primer set are listed in Supplementary Table 9.

eChIP-quantitative qPCR. The zona pellucidae of the embryos were removed by acid Tyrode's solution and washed in PBS containing 0.1% PVA. The embryos were suspended in PBS containing 0.5% Triton-X, 0.5 mM DTT and protease inhibitor, and incubated on ice for 30 min. After incubation, 1 mM $CaCl_2$ was added to the buffer and samples were incubated for 5 min at 37 °C. After incubation, 0.5 µl (2×10^6 gel units per ml) micrococcal nuclease (New England BioLabs) was added to the nuclei, which were then incubated for 5 min at 37 °C. EDTA was added to a concentration of 0.5 mM and solubilized chromatin was clarified by centrifugation at 15,000 r.p.m. for 15 min at 4 °C. The same procedures were repeated one more time. Chromatin was incubated with Protein A beads conjugated to anti-H3K9me3 antibodies (ab8898) or rabbit IgG (ab37415), prepared as described above, overnight at 4 °C in ChIP buffer (40 mM Tris–HCL, pH 7.5, 1 M NaCl and 10 mM EDTA). Pelleted beads were washed twice with Buffer 1 (50 mM Tris–HCL, pH 7.5, 500 mM NaCl and 10 mM EDTA) and then with Buffer 2 (50 mM Tris–HCL, pH 7.5, 300 mM NaCl and 10 mM EDTA). The pelleted beads were then suspended in ChIP direct elution buffer and incubated with proteinase K for 2 h at 55 °C. The immunoprecipitated DNA was then purified using Agencourt AMpure XP beads.

Eluted DNA (20 µl) was divided into two aliquots; one (4 µl) was used for a SYBR Green assay targeting a major satellite and the other (16 µl) was subjected to pre-amplification using a Single Cell-to-CT kit (Ambion, Austin, TX, USA) according to the manufacturer's instructions. The number of PCR cycles at the pre-amplification step was 20. The primer and probe sequences used are shown in Supplementary Table 9.

Microarray analysis. Five *Egfp*-PE, *Kdm4b*-PE and IVF blastocysts (120 h) were lysed using ISOGEN (Nippongene) and RNA was extracted by phenol–chloroform and isopropanol precipitation. cDNA was synthesized using the Ovation RNA Amplification System V2 kit (NuGEN, West Cumbria, UK) and hybridized with SurePrint G3 Mouse GE 8x60K Microarray (Agilent Technologies). Analysis was conducted using GeneSpringV12.5 (Agilent Technologies). Transcripts were considered to be expressed if raw values were >100 and a flag was present in at least one of the groups.

References

1. Augui, S., Nora, E. P. & Heard, E. Regulation of X-chromosome inactivation by the X-inactivation centre. *Nat. Rev. Genet.* **12,** 429–442 (2011).
2. Lee, J. T. Gracefully ageing at 50, X-chromosome inactivation becomes a paradigm for RNA and chromatin control. *Nat. Rev. Mol. Cell Biol.* **12,** 815–826 (2011).
3. Wutz, A. Gene silencing in X-chromosome inactivation: advances in understanding facultative heterochromatin formation. *Nat. Rev. Genet.* **12,** 542–553 (2011).
4. Takagi, N. & Sasaki, M. Preferential inactivation of the paternally derived X chromosome in the extraembryonic membranes of the mouse. *Nature* **256,** 640–642 (1975).
5. Shin, J. *et al.* Maternal Rnf12/RLIM is required for imprinted X-chromosome inactivation in mice. *Nature* **467,** 977–981 (2010).
6. Tada, T. *et al.* Imprint switching for non-random X-chromosome inactivation during mouse oocyte growth. *Development* **127,** 3101–3105 (2000).
7. Chiba, H. *et al. De novo* DNA methylation independent establishment of maternal imprint on X chromosome in mouse oocytes. *Genesis* **46,** 768–774 (2008).
8. Marahrens, Y., Panning, B., Dausman, J., Strauss, W. & Jaenisch, R. Xist-deficient mice are defective in dosage compensation but not spermatogenesis. *Genes Dev.* **11,** 156–166 (1997).
9. Liu, N. *et al.* Genome-wide gene expression profiling reveals aberrant MAPK and Wnt signaling pathways associated with early parthenogenesis. *J. Mol. Cell Biol.* **2,** 333–344 (2010).
10. Obata, Y. & Kono, T. Maternal primary imprinting is established at a specific time for each gene throughout oocyte growth. *J. Biol. Chem.* **277,** 5285–5289 (2002).
11. Kono, T. *et al.* Birth of parthenogenetic mice that can develop to adulthood. *Nature* **428,** 860–864 (2004).
12. Kawahara, M. *et al.* High-frequency generation of viable mice from engineered bi-maternal embryos. *Nat. Biotechnol.* **25,** 1045–1050 (2007).
13. Santos, F., Peters, A. H., Otte, A. P., Reik, W. & Dean, W. Dynamic chromatin modifications characterise the first cell cycle in mouse embryos. *Dev. Biol.* **280,** 225–236 (2005).
14. Cantone, I. & Fisher, A. G. Epigenetic programming and reprogramming during development. *Nat. Struct. Mol. Biol.* **20,** 282–289 (2013).
15. Lewis, A. *et al.* Imprinting on distal chromosome 7 in the placenta involves repressive histone methylation independent of DNA methylation. *Nat. Genet.* **36,** 1291–1295 (2004).
16. Yuan, P. *et al.* Eset partners with Oct4 to restrict extraembryonic trophoblast lineage potential in embryonic stem cells. *Genes Dev.* **23,** 2507–2520 (2009).
17. Fodor, B. D. *et al.* Jmjd2b antagonizes H3K9 trimethylation at pericentric heterochromatin in mammalian cells. *Genes Dev.* **20,** 1557–1562 (2006).
18. Nakamura, T. *et al.* PGC7 binds histone H3K9me2 to protect against conversion of 5mC to 5hmC in early embryos. *Nature* **486,** 415–419 (2012).
19. Nesterova, T. B., Barton, S. C., Surani, M. A. & Brockdorff, N. Loss of Xist imprinting in diploid parthenogenetic preimplantation embryos. *Dev. Biol.* **235,** 343–350 (2001).
20. Plath, K. *et al.* Role of histone H3 lysine 27 methylation in X inactivation. *Science* **300,** 131–135 (2003).
21. Okamoto, I., Tan, S. & Takagi, N. X-chromosome inactivation in XX androgenetic mouse embryos surviving implantation. *Development* **127,** 4137–4145 (2000).
22. Barakat, T. S. *et al.* RNF12 activates Xist and is essential for X chromosome inactivation. *PLoS Genet.* **7,** e1002001 (2011).
23. Puschendorf, M. *et al.* PRC1 and Suv39h specify parental asymmetry at constitutive heterochromatin in early mouse embryos. *Nat. Genet.* **40,** 411–420 (2008).
24. Dahl, J. A. & Collas, P. A rapid micro chromatin immunoprecipitation assay (microChIP). *Nat. Protoc.* **3,** 1032–1045 (2008).
25. Turner, B. in *Mapping Protein/DNA Interactions by Cross-Linking* (2001).
26. Hoki, Y. *et al.* A proximal conserved repeat in the Xist gene is essential as a genomic element for X-inactivation in mouse. *Development* **136,** 139–146 (2009).
27. Fukuda, A. *et al.* Identification of inappropriately reprogrammed genes by large-scale transcriptome analysis of individual cloned mouse blastocysts. *PLoS ONE* **5,** e11274 (2010).
28. Inoue, K. *et al.* Impeding Xist expression from the active X chromosome improves mouse somatic cell nuclear transfer. *Science* **330,** 496–499 (2010).
29. Marks, H. *et al.* The transcriptional and epigenomic foundations of ground state pluripotency. *Cell* **149,** 590–604 (2012).
30. Karimi, M. M. *et al.* DNA methylation and SETDB1/H3K9me3 regulate predominantly distinct sets of genes, retroelements, and chimeric transcripts in mESCs. *Cell Stem Cell* **8,** 676–687 (2011).
31. Ono, Y. & Kono, T. Irreversible barrier to the reprogramming of donor cells in cloning with mouse embryos and embryonic stem cells. *Biol. Reprod.* **75,** 210–216 (2006).
32. Dindot, S. V., Person, R., Strivens, M., Garcia, R. & Beaudet, A. L. Epigenetic profiling at mouse imprinted gene clusters reveals novel epigenetic and genetic features at differentially methylated regions. *Genome Res.* **19,** 1374–1383 (2009).
33. Sasaki, H. & Matsui, Y. Epigenetic events in mammalian germ-cell development: reprogramming and beyond. *Nat. Rev. Genet.* **9,** 129–140 (2008).
34. Sugimoto, M. & Abe, K. X chromosome reactivation initiates in nascent primordial germ cells in mice. *PLoS Genet.* **3,** e116 (2007).
35. Duszczyk, M. M., Wutz, A., Rybin, V. & Sattler, M. The Xist RNA A-repeat comprises a novel AUCG tetraloop fold and a platform for multimerization. *RNA* **17,** 1973–1982 (2011).
36. Gontan, C. *et al.* RNF12 initiates X-chromosome inactivation by targeting REX1 for degradation. *Nature* **485,** 386–390 (2012).
37. Zhang, L. *et al.* RNF12 controls embryonic stem cell fate and morphogenesis in zebrafish embryos by targeting Smad7 for degradation. *Mol. Cell* **46,** 650–661 (2012).
38. Shin, J. *et al.* RLIM is dispensable for X-chromosome inactivation in the mouse embryonic epiblast. *Nature* **511,** 86–89 (2014).
39. Brykczynska, U. *et al.* Repressive and active histone methylation mark distinct promoters in human and mouse spermatozoa. *Nat. Struct. Mol. Biol.* **17,** 679–687 (2010).
40. Hammoud, S. S. *et al.* Distinctive chromatin in human sperm packages genes for embryo development. *Nature* **460,** 473–478 (2009).

Acknowledgements

We are grateful to T. Sado for critical reading of this manuscript and discussions. We thank T. Sugawara and H. Kobayashi for helpful comments; A. Bradley for providing the PiggyBac vector; K. Kusakabe, T. Kikuchi, Y. Harada, S. Kanai and Y. Takahashi for technical assistance with some experiments and analysis; and T. Kawasaki for preparation of figures. This work was supported by grants from the Ministry of Education, Culture, Sports, Science and Technology (MEXT) of Japan; a grant from the Ministry of Health, Labour and Welfare (MHLW) to H.A. and A.U.; a Grant-in-aid for Scientific

Research (21390456); a grant from JST-CREST to H.A.; and a JSPS KAKENHI Grant-in-Aid for Research Activity Start-up to A.F. (24890300).

Author contributions

A.F., K.E. and H.A. conceived and designed the study. A.F. performed the experiments and analysis of embryo manipulation, IF, FISH, qPCR, ChIP, cultured ES cells, vector construction and microarray analysis, and developed the eChIP-qPCR technique. J.T., K.H. and K.N. conducted ChIP-seq experiments and analyses. T.M. and H.A. constructed vectors and cultured ES cells. H.A. and A.U. supervised the study. A.F., K.N. and H.A. wrote the manuscript.

Additional information

Accession codes: The original data for the microarray have been deposited in the GEO at http://www.ncbi.nlm.nih.gov/geo/ (accession number: GSE53662). The original data of ChIP-seq have been deposited in DDBJ at http://cibex.nig.ac.jp/index.jsp with accession number: DRA001041.

Supplementary Information accompanies this paper at http://www.nature.com/naturecommunications

Competing financial interests: The authors declare no competing financial interests.

Reprints and permission information is available online at http://npg.nature.com/reprintsandpermissions/

How to cite this article: Fukuda, A. *et al.* The role of maternal-specific H3K9me3 modification in establishing imprinted X-chromosome inactivation and embryogenesis in mice. *Nat. Commun.* 5:5464 doi: 10.1038/ncomms6464 (2014).

Laboratory Investigation (2015) 95, 26–42

MINI REVIEW

Generation of pluripotent stem cells without the use of genetic material

Akon Higuchi[1,2,9], Qing-Dong Ling[3,4,9], S Suresh Kumar[5], Murugan A Munusamy[2], Abdullah A Alarfaj[2], Yung Chang[6], Shih-Hsuan Kao[1], Ke-Chen Lin[1], Han-Chow Wang[7] and Akihiro Umezawa[8]

Induced pluripotent stem cells (iPSCs) provide a platform to obtain patient-specific cells for use as a cell source in regenerative medicine. Although iPSCs do not have the ethical concerns of embryonic stem cells, iPSCs have not been widely used in clinical applications, as they are generated by gene transduction. Recently, iPSCs have been generated without the use of genetic material. For example, protein-induced PSCs and chemically induced PSCs have been generated by the use of small and large (protein) molecules. Several epigenetic characteristics are important for cell differentiation; therefore, several small-molecule inhibitors of epigenetic-modifying enzymes, such as DNA methyltransferases, histone deacetylases, histone methyltransferases, and histone demethylases, are potential candidates for the reprogramming of somatic cells into iPSCs. In this review, we discuss what types of small chemical or large (protein) molecules could be used to replace the viral transduction of genes and/or genetic reprogramming to obtain human iPSCs.

Laboratory Investigation (2015) **95,** 26–42; doi:10.1038/labinvest.2014.132; published online 3 November 2014

Pluripotent stem cells (PSCs) can be derived from terminally differentiated tissues by altering the epigenetic status of cells. These PSCs have the potential to differentiate into any cell type derived from the three germ layers.[1–5] Cell type determination is heavily dependent on epigenetic process. The generation of iPCSs from differentiated cells is partly regulated by epigenetics. PSCs provide an unlimited cell source with the potential for use in studying diseases, drug screening, and regenerative medicine. Human PSCs provide a promising platform for obtaining patient-specific cells for various therapeutic and research applications. In general, induced pluripotent stem cells (iPSCs) are generated via genetic manipulation or by nuclear transfer to generate PSCs from somatic cells.[6] However, nuclear transfer-generated PSCs raised ethical concerns and are technically difficult to prepare. The genetic manipulation of PSCs limits their clinical uses. Although embryonic stem cells (ESCs) do not need to be genetically manipulated, there are strong ethical concerns regarding human ESCs (hESCs), limiting their use in clinical applications.

iPSCs were first generated in 2006–2007 by the transduction of four transcription genes, Oct3/4, Sox2, c-Myc, and Klf-4[7–10] or Oct 4, Sox2, Nanog, and Lin28.[11] Following these studies, several researchers succeeded in generating iPSCs using fewer pluripotent genes. Of note, researchers generated iPSCs without transducing c-Myc, a potent oncogene.[12–14] Currently, mouse iPSCs (miPSCs) can be generated by reprogramming a single gene, such as *Oct4*,[15,16] or with the aid of small or large molecules in place of gene transduction.[17–19] However, the low reprogramming efficiency of human iPSCs (hiPSCs) is a major drawback. The use of virus-mediated delivery of reprogramming factors, which leads to the permanent integration of oncogenes and potentially harmful genomic alterations,[20] is a serious concern. The use of genome-integrating viruses could cause insertional mutagenesis and unpredictable genetic dysfunction.[9,21]

Therefore, several reprogramming technologies that do not use viral integration have been developed for iPSC production.[22,23] These approaches include the use of non-integrating viruses,[24–26] transposon-based systems,[27] and the delivery of reprogramming factors on plasmids.[22,28–30] Adenovirus, lentivirus, Sendai virus, miRNA, and plasmid transfection methods have been reported to generate miPSCs[28,31] and

[1]Department of Chemical and Materials Engineering, National Central University, Jhongli, Taiwan; [2]Department of Botany and Microbiology, King Saud University, Riyadh, Saudi Arabia; [3]Institute of Systems Biology and Bioinformatics, National Central University, Jhongli, Taiwan; [4]Cathay Medical Research Institute, Cathay General Hospital, Taipei, Taiwan; [5]Department of Medical Microbiology and Parasitology, Universities Putra Malaysia, Slangor, Malaysia; [6]Department of Chemical Engineering, R&D Center for Membrane Technology, Chung Yuan Christian University, Jhongli, Taiwan; [7]Department of Obstetrics and Gynecology, Hungchi Women and Children's Hospital, Jhongli, Taiwan and [8]Department of Reproduction, National Research Institute for Child Health and Development, Tokyo, Japan
Correspondence: Professor A Higuchi, PhD, Department of Chemical and Materials Engineering, National Central University, No. 300, Jhongda Road, Jhongli 32001, Taiwan.
E-mail: higuchi@ncu.edu.tw
[9]These authors contributed equally to this work.

Received 16 June 2014; revised 25 July 2014; accepted 25 July 2014

hiPSCs[24,30,32–35] to minimize chromosomal disruption.[18] Yu *et al.* generated hiPSCs by transfecting non-integrating episomal vectors.[30] In addition, the piggyBac transposon[18,27,31] and Cre-recombinase excisable viruses[36] have been used to generate hiPSCs. The transgenes can be excised by inducible gene expression once reprogramming is established.[25,27,36] However, there is evidence that there can be problems with residual DNA and chromosomal disruptions, resulting in harmful genetic alterations.[18]

The repeated transfection of modified mRNA encoding the reprogramming factors is also efficient for generating iPSCs.[22,37] Although these strategies eliminate the threat of random viral integration into the host cell genome, these approaches are technically challenging and less efficient than viral transduction. Therefore, it is important to identify new conditions and small or large molecules that can promote reprogramming and ultimately replace all of the reprogramming transcription factors (TFs).[14,38–41] For clinical applications, using small or large molecules to generate PSCs are preferable to genetic manipulations. Recently, several novel methods have been reported for generation of iPSCs without the use of genetic material; these methods include protein-induced PSCs (piPSCs) that are reprogrammed from somatic cells using cell-penetrating TF proteins,[18,19] and chemically iPSCs (CiPSCs) that are reprogrammed from somatic cells using small molecules.[14,17,20,38–49]

Human CiPSCs are a promising tool in the clinical application of PSCs. CiPSCs can be reprogrammed to become iPSCs from somatic cells, without genetic manipulation, through the addition of small-molecule chemicals in the culture medium. In this review, we will discuss the generation of iPSCs without the use of genetic material and instead using small or large (protein) molecules. We will discuss types of small and/or large (protein) molecules that can replace specific viral transduction of pluripotent TFs to obtain piPSCs and CiPSCs from somatic cells.

PSCs REPROGRAMMING WITH PROTEINS (piPSCs)

In the reprogramming of somatic cells into iPSCs, one of the methods that avoids exogenous genetic introduction to the target cells is delivering the reprogramming proteins directly into cells rather than transducing the cells with TF genes. Previous researchers have reported that the proteins can be delivered into mammalian cells *in vitro* and *in vivo* by conjugating the proteins with a short peptide to guide their transduction, such as HIV transactivator of transcription (tat) or polyarginine.[30,50–52] Various solubilization and refolding techniques have been developed so that recombinant proteins expressed in *E. coli* and contained in inclusion bodies can be re-folded into bioactive proteins. This allows for easy, large-scale production of therapeutic proteins.[30,53] Currently, recombinant forms of Oct4, Sox2, Klf4, and c-Myc are commercially available. Table 1 summarizes the reprogramming of mouse and human somatic cells into piPSCs with the aid of proteins by transduction without TFs.

The challenge in delivering proteins into cells is the proteins' limited capacity to penetrate the cell membranes. Proteins that are capable of crossing the cell membrane barrier generally contain high proportions of basic amino acids, such as lysine and arginine.[54,55] and the HIV tat protein has a short, basic segment of 48–60 amino-acid residues that is known to cross the cell membrane and to activate HIV-specific genes.[18,54] In 2009, Zhou *et al.* attached a transfection domain of a polyarginine protein to the C terminus of the four reprogramming factors Oct4, Sox2, Klf4, and c-Myc to generate recombinant proteins that are able to permeate the plasma membranes of mouse embryonic fibroblasts (MEFs).[19] The mouse piPSCs that were generated were stably expanded for 30 passages, and the morphology of the piPSCs was similar to ESCs, as they formed small, compact, domed colonies.[19] The piPSCs expressed typical pluripotency markers, including ALP, SSEA1, Nanog, Oct4, and Sox2, as assayed by immunostaining. The expression of endogenous pluripotency genes was verified by RT-PCR. The piPSCs generated embryoid bodies in suspension and differentiated into cells characteristic of the three germ layers: (a) endoderm cells expressing AFP, FoxA2, GATA4, Sox17, albumin (hepatic marker), and Pdx1 (pancreatic marker); (b) mesoderm cells expressing Brachyury and mature beating cardiomyocytes expressing the CT3 and MHC markers; and (c) ectoderm cells expressing Pax5 and Sox1 (neural markers) and βIII-tubulin and MAP2ab (mature neuronal markers).[19] Although these findings are promising, the extremely low efficiency (0.006%) and poor reproducibility of the generation of piPSCs hinders its use as a general method for generating iPSCs.

The same year, Kim *et al.* reported the generation of piPSCs from human newborn fibroblasts (HNFs) using four recombinant cell-penetrating reprogramming proteins (Oct4, Sox2, Klf4, and c-Myc) fused with a cell-penetrating peptide (CPP, polyarginine with nine repeating arginine residues).[18] The authors generated HEK293 cell lines that expressed each of the four human reprogramming proteins fused to CPP. HNFs were treated with cell extracts from the HEK293 cell lines. After repeated treatment with the cell extracts containing the reprogramming proteins, the HNFs ultimately became human piPSCs.[18] The human piPSCs showed similar characteristics to hESCs (H9) in cell morphology and pluripotent marker expression and were cultured for more than 35 passages without loss of pluripotency, which suggests that the appropriate epigenetic reprogramming events occurred in these cells. The human piPSCs were successively differentiated into cells derived from the three germ layers both *in vitro* (embryonic formation) and *in vivo* (teratoma formation).[18] Interestingly, Kim *et al.* could not generate mouse piPSCs when they applied the same method to mouse cells.[18] This discrepancy might be due to a low concentration of reprogramming proteins, as they used whole-protein extracts from HEK293 cells as the source of the reprogramming proteins. Furthermore, Kim *et al.* did not add

Table 1 Reprogramming of mouse and human somatic cells into iPSCs with the aid of proteins by transduction without transcription factors (TFs)

TFs required	*Somatic cells*	*PSCs*	*Small molecules*	*Efficiency (%)*	*Reference*
Mouse					
No factor	MEFs (NIH3T3)	miMPCs	mESC (D3) extract with streptolysin O treatment	NA	60
No factor	MEFs	miPSCs	VPA, four recombinant proteins (OSKM) with polyarginine tag	0.006%	19
No factor	MEFs	miPSCs	VPA, three recombinant proteins (OSK) with polyarginine tag	0.002%	19
No factor	Mouse skin fibroblasts	miMPCs	Fish egg extract	NA	57
No factor	Mouse cardiac fibroblasts	miPSCs	mES (C57) cell line extract	0.001%	59
No factor	Mouse dermal fibroblasts	miPSCs	mES (C57) cell line extract	NA	56
Human					
No factor	Human new born fibroblasts	hiPSCs	HEK293 Cell extract containing Recombinant proteins with polyarginine tag	0.001%	18
No factor	Human NPCs derived from cord blood	hiPSCs	TSA, RG-108, reprogramming proteins (Oct4, Klf4, Sox2)	0.001%	90
No factor	Human newborn foreskin fibroblast BJ (CRL-2522)	hiPSCs (hiMPCs)	Fibromodulin	0.03%	58

small molecules to the culture medium,[18] whereas Zhou *et al.* used valproic acid (VPA) for the reprogramming to generate mouse piPSCs.[19] VPA is known to enhance the reprogramming efficiency of cells to generate miPSCs.[42]

piPSC GENERATION USING CELL EXTRACTS

Jin *et al.* also generated mouse piPSCs using cell extracts instead of viral transduction. They found that cell extracts from only specific ESC lines could promote the reprogramming of mouse dermal fibroblasts into piPSCs.[56] Therefore, the authors performed protein microarrays to characterize the proteomes of different ESC lines that can and cannot reprogram the mouse dermal fibroblast. Protein extract from the ESC line that could promote reprogramming showed high levels of proteins that regulate protein synthesis and metabolism, compared with the other ESC lines that could not promote reprogramming into piPSCs; this result suggests that there are threshold concentrations of specific synthetic and metabolic proteins that the cells must exceed to initiate reprogramming.

Several researchers have reported that, in addition to ESC extracts, other cell extracts such as fish oocyte extracts[57] or a single extracellular matrix proteoglycan of fibromodulin[58] can promote the reprogramming of human fibroblast cells into human piPSCs or induced multipotent stem cells. In most cases, the specific proteins from the extracts that drive reprogramming are unknown.[57,59,60] Furthermore, it has not yet been verified whether human piPSCs can be reprogrammed with high efficiency and high reproducibility from somatic cells incubated with extracts of hESCs or other animal cells.

COMPARISON OF hiPSCs DERIVED FROM GENETIC MATERIAL AND PROTEINS

Rhee *et al.* compared multiple hiPSC lines derived from retrovirus-based, lentivirus-based, and protein-based reprogramming to hESCs based on their capacity to differentiate into neuronal stem cells (NSCs) and dopaminergic neurons.[61] Optimized co-culturing and fine selection methods led to the efficient generation of NSCs and dopaminergic neurons from hESCs and all hiPSC lines tested, including piPSCs. NSCs and dopaminergic neurons derived from hiPSCs using lentiviral transduction showed residual expression of exogenous reprogramming genes, whereas hiPSCs derived from retroviral vectors and piPSCs did not express the exogenous reprogramming genes.[61] In addition, the virus-based iPSCs exhibited early cellular senescence and limited expansion because of apoptosis during passaging, whereas hESCs and hiPSCs exhibited unlimited expansion without cellular senescence. NSCs derived from piPSCs were grafted into rats with striatal lesions, a model of Parkinson's disease. NSC engraftment resulted in striking behavioral recovery associated with a high proportion of TH^+ (ie, dopamine-secreting) neurons, and the transplantation of NSCs rescued motor deficits. However, tumors formed when a large number of NSCs was grafted into the rats.[61] The researchers also found that fully differentiated dopamine neurons are too vulnerable to survive transplantation; therefore, almost no functional recovery and no TH^+

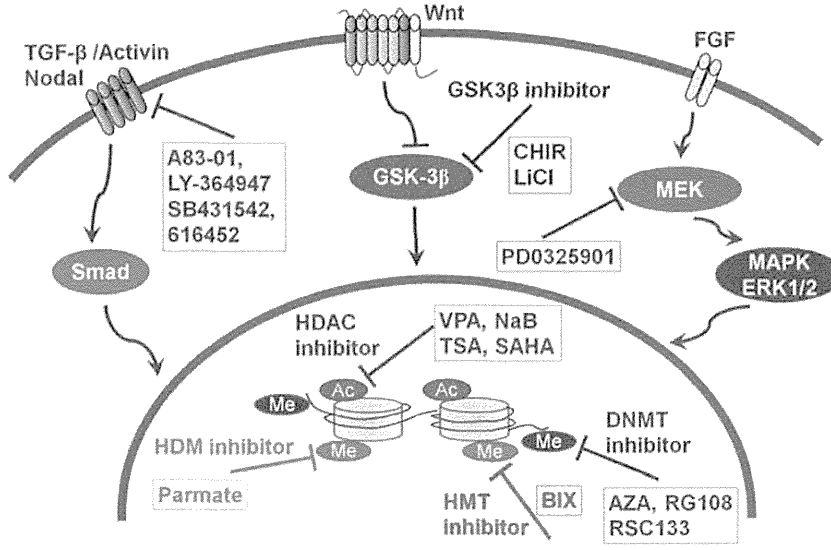

Figure 1 The signaling pathways underlying the chemical manipulation of stem cell fate and reprogramming. Epigenetic modulators can modify the chromatin structure to make it more permissive to changes in the epigenome during reprogramming. Small molecules that target signaling pathways can regulate the expression of pluripotent transcription factor genes, leading to the reprogramming of somatic cells into iPSCs. Several small-molecule inhibitors of epigenetic modification enzymes, such as DNA methyltransferases (DNMTs), histone deacetylases (HADC), histone methyltransferases (HMT), and histone demethylases (HDM) that act as major players in forming the epigenetic landscape, have been selected as small chemical molecules for the reprogramming of somatic cells into iPSCs. The abbreviations of the small molecules are shown in Table 2.

neurons were generated in their study.[61] This study elegantly described the superiority of hiPSCs generated by virus-free methods, although optimization is still required to remove residual undifferentiated cells and to avoid tumor generation. Such work will pave the way for standardized quality control before moving hiPSCs into clinical trials[62] and will support the use of human piPSCs in clinical applications, such as personalized cell therapy for specific diseases.

The success of human piPSCs opens an avenue to generate safe production protocols for hiPSCs, as human piPSCs can eliminate the potential risks from the use of viral vectors and DNA transfection. However, the extremely low efficiency of piPSC generation (approximately 0.001%) is an issue blocking the use of human piPSCs in clinical applications.

SMALL MOLECULES THAT PROMOTE iPSC PRODUCTION INVOLVING FEW TFs

Small molecules that target specific signaling pathways and/or functions are valuable chemical tools in the reprogramming of somatic cells into iPSCs. These small molecules have the potential to play extensively important roles in both evaluating the basic biology of stem cells and promoting the development of clinical approaches toward regenerative medicine. Such approaches could open the door to cell replacement therapies, which use functional homogenous cells produced under chemically defined conditions *in vitro* and the development of small-molecule drugs to stimulate the endogenous patient cells to repair themselves and regenerate.[20] Here, we review recent progress made in using small molecules to either sustain pluripotency or induce the reprogramming of somatic cells into iPSCs.

Previous studies have demonstrated that the expression of four TFs can reprogram several somatic cell types into iPSCs. Furthermore, iPSCs can be generated by viral integration of *Oct4/Sox2/Klf4* without expressing the oncogene *c-Myc*, which contributes to iPSC tumorigenicity, as determined by experiments that generated chimeras and their progeny mice.[63] For therapeutic usage, it is important to minimize the number of genes transduced into somatic cells to generate iPSCs.[64] However, decreasing the number of TFs leads to decreased iPSC generation efficiency. Therefore, several small molecules have been developed to enhance the generation efficiency of iPSCs.

Epigenetic changes are important for reprogramming somatic cells into PSCs. Therefore, several small-molecule inhibitors against epigenetic-modifying enzymes that are major players in building the epigenetic landscape,[47] such as DNA methyltransferases (DNMTs), histone deacetylases (HDACs), histone methyltransferases (HMTs), and histone demethylases, were selected for somatic cell reprogramming into iPSCs. Epigenetic modulators can modify chromatin structure and make it more permissive to transcriptional machinery during somatic cell reprogramming. Some small molecules are summarized in Figure 1, which target transcription factors that are downstream in the signaling pathways. These small molecules can regulate gene expression level of pluripotent TFs, leading to somatic cell reprogramming into iPSCs, and it will be further discussed later in this review.

Small molecules with molecular weights less than 500–800 Da can freely permeate across the cell membrane and can be used to reprogram somatic cells into iPSCs.[65] It is systematically approached to identify small molecules to replace the reprogramming TFs or to promote reprogramming efficiency. One high-throughput method used to discover small molecules is as follows. Each well on the plate is seeded with somatic cells that are transduced with Oct4 promoter-driven enhanced green fluorescence protein and subsequently transcription factors, as endogenous *Oct4* expression is the first indication that iPSCs are being generated. Next, a panel of small molecules are screened, which can either replace Sox2, Oct4, and/or promote the efficiency of reprogramming. Colony numbers expressing GFP were evaluated as read out of this experiment. The colony generation efficiency is estimated from cells treated with and without small molecules.

Table 2 shows the small molecules that can replace TFs, which are required for reprogramming and increase reprogramming efficiency in generating iPSCs. These small molecules are inhibitors of epigenetic marks and singling pathways.

SMALL MOLECULES THAT CAN REPLACE *Oct4*

Oct4 is the master regulatory pluripotency gene and may serve as a pluripotency determinant in reprogramming.[15,66–68] BIX01294, a G9a HMTase inhibitor, was reported to induce miPSCs in place of *Oct4* (Table 2).[69] Furthermore, Forskolin (FSK, cAMP agonist), D4476 (casein kinase 1 inhibitor), and 2-methyl-5-hydroxytryptamine (5-HT3 agonist) can replace *Oct4* in mouse cells with the aid of other small molecules.[17] RG108, a DNMT inhibitor, can replace *Oct4* during mouse skeletal muscle cell reprogramming into miPSCs where skeletal muscle cells endogenously express *Sox2*, *Klf4*, and *c-Myc*.[70] Figure 2 shows the chemical scheme of small molecules that may functionally replace *Oct4* and *Klf4* during somatic cell reprogramming into iPSCs.

The compounds 616452 (E-616452) and SB431542 are transforming growth factor (TGF)-β inhibitors that could replace *Sox2* during mouse and human iPSC generation (Figure 1).[15,69–71] Compound 616452 can replace *Sox2* in the MEF reprogramming. However, 616452 does not actually act by inducing *Sox2* expression in the target cells; rather, it enables reprogramming through the induction of *Nanog* transcription.[69] Another TGF-β inhibitor, LY-364947, can replace *Sox2* in miPSC generation (Figure 1).[69,72] Furthermore, the glycogen synthase kinase-3 (GSK-3) inhibitor CHIR99021 (CHIR), which activates the Wnt signaling pathway, was reported to induce the reprogramming of both mouse and human somatic cells without the use of a *Sox2* transgene.[71] The protein arginine methyltransferase inhibitor AMI-5 enables *Oct4*-induced reprogramming of MEFs in combination with the TGF-β inhibitor A83-01 (A-83-01) and can replace *Sox2* during mouse somatic cell reprogramming.[73] BayK8644 (BayK), an L-channel calcium agonist, was also reported to be able to replace *Sox2* in combination with BIX01294 during MEF reprogramming into miPSCs.[63] Shh, purmorphamine, and oxysterol, the activator of Sonic hedgehog signaling, have been reported to upregulate *Bmi1*, *Sox2*, and *N-Myc* expression in mouse fibroblasts.[74] Therefore, these molecules can replace *Sox2* in mouse fibroblast reprogramming into NSCs that are naturally expressing *Sox2*.[74]

Staerk *et al.* applied a cell-based, high-throughput chemical screening method to identify small molecules that can replace *Sox2* during mouse somatic cell reprogramming.[72] From their *Nanog* reporter-based screening, they discovered that the Pan-Src family kinase inhibitors ipyrazine, dasatinib, and PP1 could replace *Sox2* in MEF reprogramming into miPSCs.[72] Figure 2 also shows the chemical scheme of small molecules that may functionally replace *Sox2* during somatic cell reprogramming into iPSCs.

SMALL MOLECULES THAT CAN REPLACE *Klf4* and *c-Myc*

Kenpaullone has been reported as a substitute for *Klf4* in mouse cells, although the underlying mechanism is unknown.[75] Furthermore, several small molecules can increase the iPSC generation efficiency, indicating that the small molecules can replace *Klf4* and *c-Myc* during somatic cell reprogramming into iPSCs. For example, VPA (an HDAC inhibitor) improves reprogramming efficiency by more than 100-fold and enables efficient iPSC induction without the introduction of *c-Myc*.[76]

SMALL MOLECULES THAT PROMOTE THE EFFICIENCY OF iPSC GENERATION

Figure 3 shows the chemical scheme of small molecules that promote somatic cell reprogramming into iPSCs. 5-Azacytidine, which is a DNMT inhibitor is reported to facilitate the transition of partially reprogrammed MEFs into fully reprogrammed iPSCs from 0.41% in partially reprogrammed MEFs to 77.8% with 5-azacytidine treatment after five passages.[77]

The MEK inhibitor PD0325901 can inhibit the mitogen-activated protein kinase/extracellular signal-regulated kinase signaling pathway to promote late somatic cell reprogramming into mouse and human iPSCs (Figure 1).[20,67,71] PD0325901 enhances the efficiency and completion of the iPSC reprogramming process. PD0325901 inhibits the growth of non-iPSC colonies and promotes the growth of reprogrammed iPSCs, leading to larger and more homogeneous iPSC colonies.[67]

Tranylcypromine (brand name: Parnate), an H3K4 demethylation inhibitor, can also promote the reprogramming efficiency of mouse somatic cells into miPSCs (approximately 20-fold).[15] Tranylcypromine is also known to activate endogenous *Oct4* expression in mouse embryonic carcinoma cells.[78]

Sodium butyrate, a natural small fatty acid and HDAC inhibitor, increases the efficiency of mouse and human iPSC

Table 2 Small molecules facilitating somatic cell reprogramming and their function

Small molecules	*C*[a]	*Host animal*	*Function*	*TFs to be replaced or function*	*Reference*
5-aza-CR, AZA	0.5 mM	Mouse	DMNT inhibitor	Promotion of reprogrammming	77
RG108	0.04–500 μM	Mouse	DMNT inhibitor	Sox2 (with BIX) or Oct4	63
RSC133	10 μM	Human	DMNT inhibitor, Histone deacetylase inhibitor	Promotion of reprogramming	82
Sodium butyrate	0.5–1 mM	Mouse, human	HDAC inhibitor	Promotion of reprogramming	79
SAHA	5 μM	Mouse	HDAC inhibitor	Promotion of reprogramming	42
TSA	20 nM	Mouse	HDAC inhibitor	Promotion of reprogramming	42
VPA	0.5–2 mM	Mouse, human	HDAC inhibitor	Promotion of reprogramming	15
Tranylcypromine (Parnate)	5–10 μM	Mouse	H3K4 demethylation inhibitor (epigenetic modulator)	Promotion of reprogramming	71
BIX	0.5–2 μM	Mouse	G9a HMTase inhibitor	Oct4	67
CHIR	3–10 μM	Mouse, human	GSK-3β inhibitor that activate Wnt signalling pathway	Sox2	15
Kenpaullone	5 μM	Mouse	GSK-3/CDKs inhibitor	Klf4	75
Compound B6	1 μM	Mouse	AKt-mediated inhibitor of GSK3-β	Promotion of reprogramming	84
LiCl	5–10 mM	Mouse and human	GSK-3β inhibitor, LSD1 inhibitor	Promotion of reprogramming	70
616452 (E-616452, RepSox)	1 μM	Mouse, human	TGF-β inhibitor (ALKinhibitor II)	Sox2	69
A83-01	0.5 μM	Mouse, human	TGF-β inhibitor	Promotion of reprogramming	43
LY-364947	1 μM	Mouse	TGF-β inhibitor	Sox2	72
SB431542	2 μM	Mouse, human	TGF-β inhibitor	Promotion of reprogramming	71
PD0325901 (PD)	0.5–1 μM	Mouse, human	MEK inhibitor	Promotion of reprogramming	67
AMI-5	5 μM	Mouse	Protein arginine methyltransferase inhibitor	Sox2, Klf4 (with A-83-01)	73
N-oxaloylglycine	1 μM	Human	Prolyl-4-hydroxylase inhibitor	Promotion of reprogramming	43
Compound B4 (TGFb-RI)	1 μM	Mouse	ALK4 inhibitor	Promotion of reprogramming	84
Dasatinib	0.5 μM	Mouse	Src family tyrosine kinase inhibitor	Sox2	72
iPY razine (iPY)	10 μM	Mouse	Src family tyrosine kinase inhibitor	Sox2	72
PP1	10 μM	Mouse	Src family tyrosine kinase inhibitor	Sox2	72
Rapamycin	0.3 nM	Mouse	mTOR inhibitor	Promotion of reprogramming	83
Compound B8	1–2 μM	Mouse	IP3K inhibitor	Promotion of reprogramming	84
Compound B10	1–2 μM	Mouse	P38 kinase inhibitor	Promotion of reprogramming	84
D4476	5 μM	Mouse	CK1 inhibitor	Oct 4 with FSK and 2-Me-5HT	17
BayK	2 μM	Mouse	a L-channel calcium agonist	Sox2	63
FSK	10–50 μM	Mouse	cAMP agonist	Oct4 with 2-Me-5HT), and D4476	17
Prostaglandin E2	5 μM	Mouse	cAMP agonist	Promotion of reprogramming	17
Rolipram	10 μM	Mouse	cAMP agonist	Promotion of reprogramming	17
2-Me-5HT	5 μM	Mouse	5-HT3 agonist	Oct4 with FSK and D4476	17
5-(4-Chloro-phenyl)-3-phenyl-pent-2-enoic acid (PS48)	5 μM	human	PDK1 activator	Promotion of reprogramming	43
8-Br-cAMP	0.1–0.5 mM	Human	cAMP-dependent protein kinase activator	Promotion of reprogramming	65
Fructose 2,6-bisphosphate	10 mM	Human	Phosphofructokinase 1 activator	Promotion of reprogramming	43
Quercetin	1 μm	Human	Hypoxia-inducible factor pathway activator	Promotion of reprogramming	43